Brain Structure and Function (2019) 224:2247–2267
https://doi.org/10.1007/s00429-019-01863-3

ORIGINAL ARTICLE

# On the existence of mechanoreceptors within the neurovascular unit of the mammalian brain

Jorge Larriva-Sahd[1] · Martha León-Olea[2] · Víctor Vargas-Barroso[1] · Alfredo Varela-Echavarría[1] · Luis Concha[1]

Received: 30 November 2018 / Accepted: 16 March 2019 / Published online: 12 June 2019


## Abstract

We describe a set of perivascular interneurons (PINs) with series of fibro-vesicular complexes (FVCs) throughout the gray matter of the adult rabbit and rat brains. PIN–FVCs are ubiquitous throughout the brain vasculature as detected in Golgi-impregnated specimens. Most PINs are small, aspiny cells with short or long (> 1 mm) axons that split and travel along arterial blood vessels. Upon ramification, axons form FVCs around the arising vascular branches; then, paired axons run parallel to the vessel wall until another ramification ensues, and a new FVC is formed. Cytologically, FVCs consist of clusters of perivascular bulbs (PVBs) encircling the precapillary and capillary wall surrounded by end-feet and the extracellular matrix of endothelial cells and pericytes. A PVB contains mitochondria, multivesicular bodies, and granules with a membranous core, similar to Meissner corpuscles and other mechanoreceptors. Some PVBs form asymmetrical, axo-spinous synapses with presumptive adjacent neurons. PINs appear to correspond to the type 1 nNOS-positive neurons whose FVCs co-label with markers of sensory fiber-terminals surrounded by astrocytic end-feet. The PIN is conserved in adult cats and rhesus monkey specimens. The location, ubiquity throughout the vasculature of the mammalian brain, and cytological organization of the PIN–FVCs suggests that it is a sensory receptor intrinsic to the mammalian neurovascular unit that corresponds to an afferent limb of the sensorimotor feed-back mechanism controlling local blood flow.

**Keywords** Receptor · Blood vessels · Perivascular organ · End-foot · Central blood flow

## Introduction

The mechanisms regulating cerebral blood flow pertain to both basic and applied neuroscience. In this broad context, homeostatic blood supply to active areas of the brain depends upon a complex neurovascular response. Two interrelated mechanisms provide a continuous and adjusting perfusion, namely, constant cerebral blood flow over a wide range of arterial pressures and local functional hyperemia (Idecola and Nedergaard 2007; Filosa et al. 2016). Arterial blood pressure results from the orchestrated action of the cardiac output, blood viscosity, and muscular tone of the arteries to maintain it within a physiological range. This dynamic process is monitored by mechano- and chemo-receptors associated with large arteries, which decode both blood pressure and composition. Central convergence of peripheral receptors onto ganglion cells and then onto cranial nerve nuclei results in adaptive endocrine-vegetative motor responses (Hall 2016). Distally, functional hyperemia results from the coordinated actions of arterioles and arterial capillaries with the neighboring glial and neural elements, which comprise the neurovascular unit (NVU) (Roy and Sherrington 1890). While a consensus about the synergistic involvement of the vascular, glial, and neural elements in detecting functional hyperemia has been achieved, researchers have not clearly determined how mechanical or chemical information from the blood flow is transduced

**Electronic supplementary material** The online version of this article (https://doi.org/10.1007/s00429-019-01863-3) contains supplementary material, which is available to authorized users.

✉ Jorge Larriva-Sahd
jlsneuro@unam.mx

[1] Departmento de Neuroiologia del Desarrollo y Fisiología, Instituto de Neurobiología. Campus Juriquilla, Universidad Nacional Autónoma de México, Boulevard Universitario 3001, 76230 Juriquilla, Querétaro, Mexico

[2] Departmento de Neuromorfología Funcional, Instituto Mexicano de Psiquiatría "Ramón de la Fuente Muñiz", Av. México Xochimilco 101, Delegación Tlalpan, 14370 México DF, Mexico

to produce an eventual vasomotor feedback response (see Busse and Fleming 2003; Zonta et al. 2003; Idecola 2004; Filosa et al. 2016). The distinct group of cortical interneurons displaying nitric acid diaphorase (NADPH-p) and neuronal nitric oxide-synthase-immunoreactivity (nNOS-I) are relevant to the present study (Sandel 1986; Estrada and DeFelipe 1998; Vaucher et al. 2000; Ducheim et al. 2012). Interestingly, axons of a group of cortical NADPH-p interneurons distribute around cortical blood vessels suggesting that these cells are implicated in local mechanisms controlling functional hyperemia (Estrada and DeFelipe 1998; Ducheim et al. 2012). Furthermore, because nNOS-I neurons in the myenteric plexus are selectively activated by colonic elongation, they have been termed mechanoreceptor neurons (see Smith et al. 2007). However, in the absence of cellular substrate(s)-transducing mechanical cues to receptor potentials from the blood stream to the neighboring neural parenchyma (Idecola 2004; Filosa et al. 2016), a systematic search for such substrate is required. The Golgi technique has revealed a unique group of small perivascular interneurons (PINs) associated with arterial blood vessels throughout the brain parenchyma. A set of PINs extends long axons that proceed in countercurrent direction along the arterial blood vessel, organized into fibro-vesicular complexes (FVCs) that encircle the roots of tributary blood vessels. Vascular interactions and immunohistochemical characteristics of the PINs match those described previously for the type-I nitrergic interneuron (Barone and Kennedy 2000; Suárez-Sola et al. 2009). A combination of electron microscopy observations and 3D reconstructions of sites of blood vessel ramification revealed that the FVC is composed of perivascular bulbs (PVBs) encased by astrocytic end-feet (EF) and capillary basal laminae. This association coupled with the membrane-bound organelles in the PVB resemble that of the Meissner corpuscle and other mechanoreceptors (Andres and During 1973; Chouchkov 1973; Hashimoto 1973; Ide et al. 1987), suggesting that the PIN–FVCs are involved in decoding mechanical cues arising from the arterial and capillary blood flow in the brain. Immunocytochemical staining for putative neurotransmitters and 3D interactions between these presumptive receptors will be presented separately.

## Materials and methods

### Animals

Adult rats, rabbits and mice raised in our specific pathogen-free vivarium were utilized in the present study. Animal manipulations and sacrifices were done following ethical policies defined by our ad hoc Animal Research Committee.

### Rapid-Golgi technique

Brains from normal adult Wistar albino rats ($n = 250$) and New-Zealand rabbits ($n = 40$) raised in our vivarium were studied. Following sacrifice with barbiturate overdose, brains were removed from the skull and transversely cut into four quarters with a pair of sharp scissors. Rabbit tissue blocks approximately 4 mm in thickness were sampled from the brainstem; cerebellum; frontal, parietal, and occipital isocortices; hippocampus–entorhinal cortex; diencephalon; basal ganglia; olfactory cortex; olfactory bulb; and olfactory peduncle. To define species conservation of the neuron type described in the present study, specimens from adult cats ($n = 3$) and rhesus monkeys ($n = 2$) cerebral cortex from our archives were used. Regardless of the species, each block was placed in an aqueous solution containing 0.25% osmium tetroxide and 3% potassium dichromate for 10–13 days and transferred to a 0.75% silver nitrate solution for further incubation for 7 days. Tissue blocks were encased with a paraffin shell and serially sectioned at a thickness of 150 microns with a sliding microtome. Sections were transferred to 70% ethyl–alcohol, dehydrated, cleared with Terpineol–xylene, mounted, numbered, and coverslipped with Entellan (Merck). Additional specimens obtained from adult cats ($n = 4$) and rhesus monkeys ($n = 2$) from our archives were used to define species conservation of the neuron type described herein. Images were obtained with a camera lucida adapted to an Axioplan 2 (Zeiss, Oberkochen) light microscope, using 40X and 100X oil objectives. Then, Indian ink and soft pencil replicas from both species provided representative images. Somatic, axonal, dendritic, and vesicular structures were measured in digital images acquired with an AxioCam camera using Kontron software (Zeiss, Oberkochen). Since neurons described here do not fulfil the structural criteria that apply for typical projecting and short-axon neurons (Ramón y Cajal 1904), the following normative foundations were used to identify their processes (Online resource, Fig. 1). Dendrites were defined as short, varicose processes with sparse but typical dendritic spines. Axons consisted of single branches arising from the opposite cell pole of the perikaryon. The stem axon either ramified locally around the underlying blood vessel or coursed along the vascular wall. In the latter case, the axon was long (> 50 microns) until it branched dichotomously. The arising paired fibrils extended long, thin recurrent fibrils. A signature feature of the PIN's axon was that it produces numerous vesicular formations surrounding the adjacent vascular ramification. An additional characteristic of the daughter

axonal fibers was their association with large, egg-shaped excrescences at highly variable intervals. Thin recurrent fibrils were frequently observed. Although both the axon and dendrites presented conspicuous varicosities, those observed in axons exhibited a wider range of diameters. Arterial and venous blood vessels were characterized in serial sections allowing the observer to track most of small-to-medium-sized blood vessels to their corresponding tributaries at the pial or ventricular surface of the brain within the observed or adjacent section(s). Large arteries and veins were easily identified in this region. Since brains intended for Golgi impregnation were fixed by immersion, arteries appeared to have a round-shaped cross section, which contrasted with the corresponding overall elliptical shape of veins and venous sinuses. Under the electron microscope, structural criteria recommended by Maynard et al. (1957) for the identification of capillaries, arteries or veins were used.

## Immunohistochemistry and histochemistry

The primary antibodies (Table 1) were used for calcitonin gene-related peptide (CGRP) (Alvarez et al. 1993; Ishida-Yamamoto et al. 1998; Johansson et al. 1999; Warfvinge and Edvisson 2017) and vesicular glutamate co transporter 1 (VGlut1) (see Bewick 2015). For immunohistochemistry, rat brain sections were incubated for 16 h in polyclonal antibody for CGRP (1:1000) and VGlut 1 (1:5000) dissolved in 0.1 M phosphate buffer (PB). Immunoreactive sites were revealed with the ABC kit according to the previously described protocol (Vargas-Barroso and Larriva-Sahd 2013; Varela-Echavarría et al. 2017). Another set of sections was sequentially immersed in a secondary anti-rabbit Cy5 antibody diluted 1:1000 in PB 0.8% saline (PB-S) for 2 h (Table 2). Following a 5-min wash in PBS, sections were incubated in DAPI diluted 1:4000 for 5 min and mounted in Mowiol medium. Supplemental adult rat sections were separately

**Table 1** Antisera and reagents for immuno- and histofluorescence staining

| | | Primary antibodies | | | |
|---|---|---|---|---|---|
| Name | Host | Clonality | Dilution | ID* | Manufacturer |
| CGRP | Mouse | Monoclonal | 1:300 | Ab81887/ AB_1658411 | Abcam |
| VGlut1 | Guineapig | Polyclonal | 1:300 | Ab5905/ AB_2301751 | Millipore/Merck |
| nNOS | Rabbit | Polyclonal | 1:300 | Cat 24431 | Sigma Chemical Co |
| GABA | Rabbit | Polyclonal | 1:500 | A2052/ AB 477652 | Sigma-Aldrich |
| NPY | Rabbit | Polyclonal | 1:500 | Ab30914/ AB 1566510 | Abcam |
| Somatostatin | Rabbit | Polyclonal | 1:1500 | Sc13099/ AB_2195930 | Santa Cruz Biotechnology |
| Calbindin | Rabbit | Polyclonal | 1:500 | Ab1778/ AB_2307443 | Jackson ImmunoResearch Lab |

*CGRP* calcitonin-related gene protein, *sNOS* neuronal nitric oxide synthase, *VGlut 1* vesicular glutamic acid cotransporter 1

*Antibody Registry, http://antibodyregistry.org/search?q=Ab5905

**Table 2** Secondary antibodies

| | | Secondary antibodies | | | | |
|---|---|---|---|---|---|---|
| Name | Host | Fluorophore | EX/EM (nm) | Dilution | ID* | Manufacturer |
| Anti-mouse | Goat | Alexa Fluor 350 | 345/440 | 1:1000 | A--11045 AB_142754 | Molecular Probes |
| Anti-mouse | Donkey | Alexa Fluor 594 | 590/617 | 1:1000 | Ab150112 | Abcam |
| Anti-Guinea pig | Goat | Cy3 | 552/565 | 1:1000 | Ab102370 AB_10711466 | Abcam |
| Antisheep | Donkey | Alexa Fluor594 | 590/617 | 1:1000 | Ab150180 AB_2716768 | Abcam |
| Anti-rabbit | Donkey | Alexa Fluor488 | 555 | 1:300 | A 31572 | Invitrogen Co |

*Antibody Registry http://antibodyregistry.org/search?q=Ab5905

incubated with a primary antibody to nNOS. Following 16 h of incubation with the primary antibodies (Table 1), rat brain sections were incubated with the secondary antibody bound with Alexa fluor 555. Since in subsequent observations of the perivascular neurons described in the present study, they appear to correspond to the type-I nitrergic interneurons described by other researchers (see Barone and Kennedy 2000; Suárez-Sola et al. 2009), additional incubations with primary antibodies against GABA (1:500), NPY (1:500), Somatostatin (1:1500), and Calbindin (1:500) (Table 1) were performed. Following incubation with primary antibodies, sections were rinsed in PB and incubated for 16 h with anti-rabbit biotinylated secondary antibodies (Table 2) dissolved in PB. After a brief washing, sections were incubated with the ABC kit to reveal immunoreactive sites, mounted and coverslipped with Entellan (Merk).

For histochemistry, three additional adult rats ($n=3$) were anesthetized and perfused (see above) with 4% paraformaldehyde dissolved in 0.1M PB. Brains were sectioned at 40 microns with a vibratome and transferred to PB (see Varela-Echavarria et al. 2017). A set of sections was processed for NADPH-d staining and to visualize the B4 isolectin (IB4) (Table 3) which labels unmyelinated fibers (Silverman and Kruger 1990; see; Eftekhari and Evinsson 2011). Floating sections were first immersed in a PB solution containing 0.1% Triton X-100 for 5 min, then transferred to a solution of 0.1 mg/ml nitro blue tetrazolium and 1 mg of β-NADPH dissolved in PB and incubated for 45 min at room temperature. Following a rapid transfer to fresh PB, sections were mounted on glass slides, air-dried and coverslipped (Sánchez-Islas and León-Olea 2001).

Observations and image acquisition were performed using a Zeiss 780 LSM confocal microscope. Confocal digital micrographs were acquired at a 0.30 µm intervals and a resolution of 1024 × 1024 pixels and were further processed and edited with Image J and Adobe Photoshop software. The 3D images used in the illustrations were obtained with the Amira software.

### Electron microscopy

Ten male albino rats ($n=5$) were processed for routine electron microscopy as described elsewhere (Larriva-Sahd 2006). Each animal was anesthetized and sacrificed with an overdose of sodium pentobarbital (i.e., 30 mg/kg). Following perfusion through the left ventricle with 250 ml of 2.5/4% glutaraldehyde/paraformaldehyde dissolved in 0.1M sodium cacodylate buffer, the brain was manually sectioned along the coronal plane and sampled according to the Swanson atlas (Swanson 2004) as follows: parietal cortex: Level (L) 7, horizontal ($H$) = 2.1 to 3.0 and vertical ($V$) = 0.8 to 2.0; frontal cortex: L8. $H=1.0$ to 2.8, and $V=1.0$ to 3.0; piriform cortex: L2. $H=4.3$ to 6, and $V=9.6$ to 10.2; anterior thalamus: L27. $H=1.0$ to 3.9, and $V=4.2$ to 7; posterior thalamus: L33, $H=0.5$ to 4.5, and $V=4.5$ to 8.0; and olfactory bulb medulla: L3. $H=0.8$ to 1.2, and $V=4$ to 5.6. Tissue slices were postfixed with 1% osmium tetra-oxide dissolved in the same buffer for 1 h, dehydrated in acetone and flat-embedded in Epon. For light microscopy, 1-µm-thick sections were obtained with a Leica microtome equipped with glass knives and stained with an aqueous solution containing 0.5% toluidine blue. Vascular areas were identified under the light microscopy, and then the surface of ultrathin sections was reduced to include capillaries arising from larger (> 80 µm in diameter) arteries for electron microscopy observations. Ultrathin sections (60 to 70 nm) were mounted in single-slot copper grids that were previously covered with Formvar film. A JEOL 1010 electron microscope operated at 80 kV and equipped with a Gatan digital camera was used to capture images. Following the ultrastructural identification of FVCs associated with the capillary wall, the tissue blocks were serially sectioned with a Leica microtome using a diamond knife. The 3D reconstructions were performed using digital micrographs obtained from a series of 50–250 sections that were first aligned with the Fuji software and then assembled with the Reconstruct software (http://synapses.clm.utexas.edu/tools/reconstruct/reconstruct.stm). Two–five reconstructions per brain area were obtained. Additional palmar and digital skin samples from the anterior limb were examined to asses organelle homology between the vesicular structures described in the present study and the structures of peripheral mechanoreceptors.

## Results

### Rapid-Golgi technique

This section provides an account of the general features of PINs whose axons form FVCs throughout the gray matter in the brain and brainstem of adult rats and rabbits. Due to the superior impregnation obtained from rabbit specimens,

**Table 3** Reagents for histochemistry

| | | | Lectin | | | | |
|---|---|---|---|---|---|---|---|
| Nam | Full name | Species | Conjugate | EX/EM | Dilution | Product | Manufacturer |
| IB4 | Isolectin GS (IB4-Cy5) | Griffonia Simplicifolia | Cy5 | 650/668 nm | 1:80 | 132450 | Invitrogen |

**Table 4** Golgi technique

| | sPIN | psPIN | bPIN | pPIN |
|---|---|---|---|---|
| Isocortex | 5 | 5 | 4 | 4 |
| Hippocampus | 5 | 4 | 3 | 3 |
| Thalamus | 3 | 5 | 3 | 3 |
| Piriform cortex | 6 | 4 | 4 | 5 |
| Midbrain | 1 | 2 | 1 | 1 |
| Pons | 3 | 1 | 3 | 1 |
| Medulla | 2 | 1 | 3 | 1 |
| Cervical spinal cord | 1 | – | 3 | – |
| Total = 90 | 26 | 22 | 24 | 18 |

Numbers, subtypes, and distribution of perivascular neurons in the adult rabbit central nervous system

*PIN* perivascular neuron, *b* bipolar, *p* polygonal, *ps* pseudomonopolar, *s* spindle-shaped

neuronal classification and axonal specializations are described in this species (Table 4); qualitative differences with respect to the rat specimens are highlighted. The species conservation of the PINs was assessed in additional specimens of cerebral cortex of the adult cat and monkey (Online resource, Fig. 2).

The PIN's soma is typically located at sites of ramification of blood vessel or, less commonly, along the shaft of the blood vessel throughout the central nervous system (CNS) (Table 4). A defining characteristic of the PIN is that both the soma and its processes are distributed within the perivascular domain. The somata may be spindle-shaped, bipolar, pseudomonopolar, or polygonal, in descending order of frequency (Table 4). Spindle-shaped PINs (Figs. 1, 2a–e) exhibit a narrow perikaryon and extend a long axon and a rudimentary dendrite in the opposite direction. After a short trajectory (< 50 µm), the parent axon divides into paired or twin fibers, each usually producing thin, recurrent branches. A striking characteristic of twin fibers is that upon ramification of the blood vessel, one or both fibrils sprout into an FVC that distributes within the parent and root of the arising blood vessel (Figs. 1a–c, 2a–e). Distal from the site of vascular forking, the FVC converges into twin fibrils that continue until the blood vessel ramifies again and another FVC is formed. Implicitly, the abundance of twin fiber-FVCs varies as a function of both the frequency of vascular forking and the degree of parallelism between the blood vessel and the plane of the section. In privileged sections twin fibers may be traced until they resolve into discrete tuberosities underneath the pial–parenchymal interphase, the so-called Virchow–Robin space (see Jones 1970). Hence, the complete structure of the spindle-shaped PIN and its axon was visualized in the cerebral isocortex (Fig. 2a–e, h), hippocampus (Fig. 4a–d), olfactory bulb (not shown), and basal ganglia (Fig. 1), where long arteries follow a straight trajectory (Zhang et al. 2018). Elsewhere, in the cervical spinal cord (Online resource, Fig. 3), or brainstem (Figs. 2f, g, 4e, f) (Online resource, Fig. 4), the blood vessels are shorter or exhibit undulating paths; hence, only parts of the spindle-shaped and bipolar PINs are accessible to the observer (1). The bipolar PIN soma also lays at the mesangial interstitium and extends short processes that distribute around the perikaryon (Fig. 2f). Commonly, the bipolar cell axon ramifies at less than < 40 µm from its origin producing FVCs that surround the wall of one or two capillaries and a single short (< 70 µm) dendrite with occasional spines. The third set of PINs (Fig. 2g) has a rounded, egg-shaped soma extending a single short process (< 30 µm). This solitary process divides into an axon and a dendrite. The simplicity of the rounded perikaryon originating a single processes mimics ganglion cells in the peripheral nervous system and brainstem (Ramón y Cajal. 1904). The last PIN subtype or polygonal PIN is characterized by its relatively large perikaryon, 2-4-, varicose dendrites and an axon that prematurely extends collaterals within the underlying mesangium. The polygonal PIN differs from the previous subtypes in that the axon generates a larger and more elaborated FVC along the underlying blood vessel and its arising tributaries (Fig. 2h). Distally (i.e., beyond the vascular forking), the FVC reorganizes into twin fibers (Fig. 2h, asterisks) coursing along the vascular shaft, similar to those described above for the spindle-shaped PIN. The PIN somata and proximal processes were also identified in the cerebral cortex of the adult cat and monkey (Online resource, Fig. 2). In these species, PINs organize rows of cells along the vessel wall (Online resource, Fig. 2a), resembling the pattern described for the cat NADPH-positive neurons surrounding meningeal blood vessels in a previous study (Estrada et al. 1993).

Twin fibers organize FVCs. The length of twin fibers varies extensively, but they are still observed in six- or seven-order ramifications in the gray matter of the cerebral isocortex, basal ganglia, and anterior olfactory nucleus, or elsewhere until the capillary diameter decreases to less than 15 microns in the thalamus or brainstem (Online resource Fig. 4) (1). Importantly, the PIN and all its processes are partly or completely embedded in EF (vide infra). As shown in a video (Online resource, Fig. 2a, and Video 1), this location becomes obvious when the specimen is in and out of focus, revealing that the distribution of the PIN processes matches the astrocyte processes. Presumptive motor fibers identified in pial and parenchymal blood vessels display a relatively uniform structure. They are composed of round, small-to-medium-sized vesicles, united by a thin fibril that, unlike the PIN processes, lies within the wall of the blood vessel (Fig. 3c, d).

(1) Visualization of the long (> 1 mm) axon and twin fibrils of a PIN–FVC requires oil immersion (40–100x)

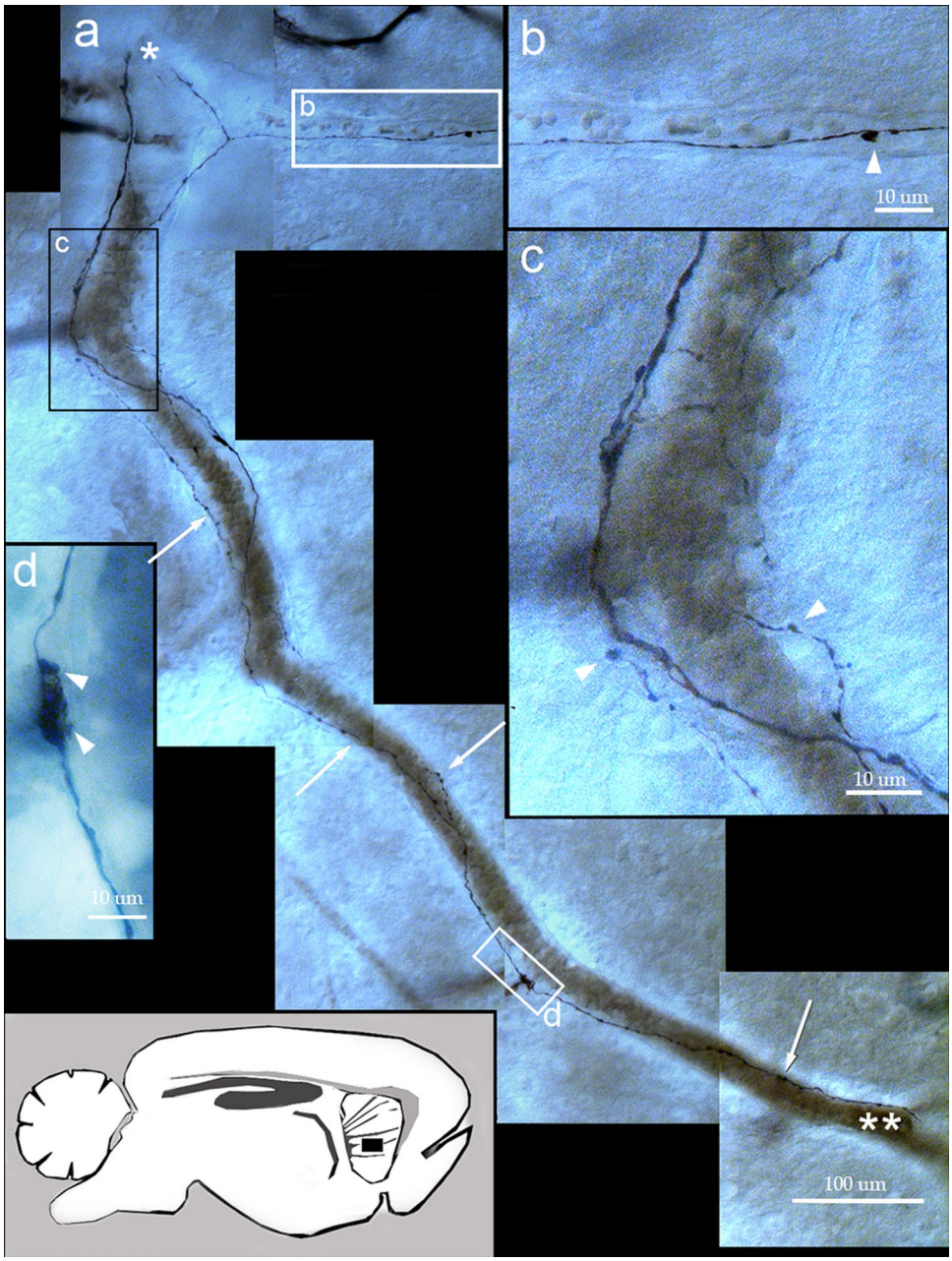


**Fig. 1** Parasagittal section of the rat caudate putamen showing perivascular neurons and twin, helicoidal fibrils following a branch of the medial striated artery (extreme upper left panel). **a** Photomontage of the artery proceeding from the subventricular neuropil (asterisk) into the basal ganglia. A perivascular neuron (framed in **d**) issues long ascending fibrils that travel helicoidally around the blood vessel (arrows), from distal (double asterisk) to superficial (asterisk) regions. **b** High-magnification images of the collateral boxed in **a**. The alternating, varicose appearance of the collateral fibril is interrupted by a balloon-like protrusion (arrowhead). Note the underlying capillary blood vessel harboring brownish, stacked red blood cells. **c** The ramification of the blood vessel coexists with collaterals of the paired axons producing rounded outgrowths of assorted sizes united by thin fibrils (arrowheads). **d** Soma and proximal processes of a spindle-shape neuron extending divergent processes. As shown in **a** the ascending axon provides daughter, twin fibrils that originate the plexus enlarged in **c** and resolve at the root of the blood vessel (asterisk). Image of the adult rat brain impregnated with Rapid-Golgi technique. Arrowheads = astroglial processes. Scale bars = 100 µm in **a**, 20 in **b** and **c**

observations and a thorough sampling of the brain (see Larriva-Sahd 2008).

Twin fibers correspond to unmyelinated axons that run separately and have dissimilar calibers. In deep blood vessels the thicker fibril measures 0.5–1.2 µm in diameter, whereas its partner fibril is 0.1–0.4 µm in diameter. Both fibrils become progressively thinner as the underlying blood vessel proceeds towards the surface of the brain or brainstem parenchyma. However, at a distance of 100–200 µm before resolving at the pia–brain interphase, the diameters of twin fibers increase progressively in diameter to resolve as a discrete enlargement (Figs. 1a, asterisk, 2e, arrowheads). As shown in the panels of Figs. 1a, c, 2b, e, paired fibers do not display uniform diameters as distinct enlargements alternate with the shaft proper. A peculiar feature of these axons is that as soon as the companion artery (see Marin-Padilla 2012) ramifies, each fibril divides into two or three branches that form a network around the roots of daughter vessels, forming the complex structure termed here FVC (Figs. 1c, 2c–e, 3e, 4). As the observer proceeds distally from the vascular forking, fibrils of the FVC converge into a new set of paired, thinner twin fibers that proceed until the blood vessel ramifies once again (Figs. 1, 2a–e). This alternating pattern persists in successive ramifications and ceases when the capillary blood vessel diameter narrows less than 15 µm.

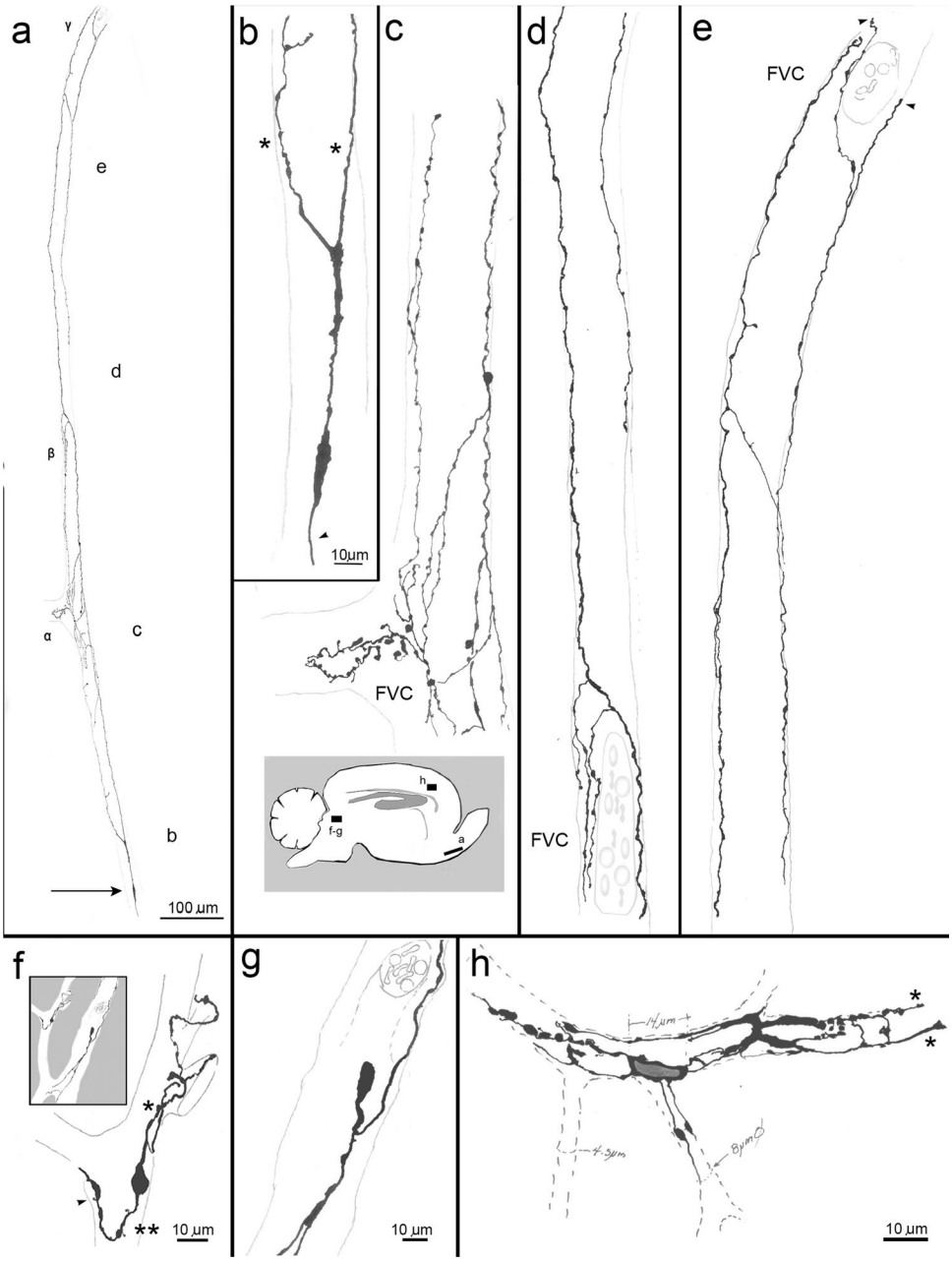


**Fig. 2** Camera lucida drawings of perivascular neurons (PIN) and their processes in the adult rabbit brain. **a** Spindle-shaped neuron (arrow) whose axon parallels a long, horizontal vessel traversing the anterior olfactory nucleus. α, β, and γ designate successive sites of the blood vessel ramification. Note the position of the cell body at the distal part of the blood vessel, and the axon and ascends against the blood flow, which presumptively courses inversely from top to bottom. **b** High-magnification image displaying fine structural features of the spindle cell perikaryon with a divergent proximal axon providing twin collaterals (asterisks) and a single dendrite (arrowhead). **c–e S**equentially enlarged images of the full axon shown in **a**. Note the fibro-vesicular complexes (FVC) that formed as twin fibrils reached the sites of the vascular ramification. **f** A bipolar type of PIN whose axon (asterisk) forms an FVC at the root of an adjacent blood vessel. The neuron extends a short, varicose dendrite (double asterisk) with sparse spines (arrowhead). **g** A pseudomonopolar PIN. Notice that the axon gives rise to a fibro-vesicular complex surrounding the vascular bifurcation, whereas the dendrite diverges into branches shortly afterwards. **h** A stellate-shaped perivascular neuron. Note the short, varicose dendrites (left side) with sparse spines, and the FVC (right side) converging into twin fibrils (asterisks)

Occasional FVCs are also seen along the vascular shaft (Online resource, Fig. 4c). Species-specific differences are noted. A first peculiarity is that the rabbit's twin fibers may undergo fasciculation so that thinner (< 1 µm) and tightly packaged fibrils are observed in high-magnification images (Fig. 4e, f). Fasciculation is noticeable immediately before a twin fiber produces an FVC. A second obvious difference noticed in the rabbit FVC, is its overall grater complexity, as it exhibits more fibrils and larger associated PVBs. Based on the complexity, the rat FVC appears to be the trimmed version (Figs. 3b, 4a–d) of the rabbit FVC (Figs. 3e, 4e, f).

In the previous description images of the frontal, parietal and piriform cortices, as well as basal ganglia, thalamus and midbrain, have been used to highlight PINs and their processes. Representative images of the medulla oblongata and cervical spinal cord are available in the Online resources, Figs. 3 and 4, respectively.

## Histochemistry and immunohistochemistry

Due to the different structures and topographies identified for the twin fiber-FVCs and the presumptive motor fibers and nerve endings associated with cerebral blood vessels (Fig. 3c, d) (Hartman et al. 1972; Cohen et al. 1997; Cauli et al. 2004; Hamel 2004; Cubelos et al. 2005), we hypothesized that the former may correspond to sensory endings

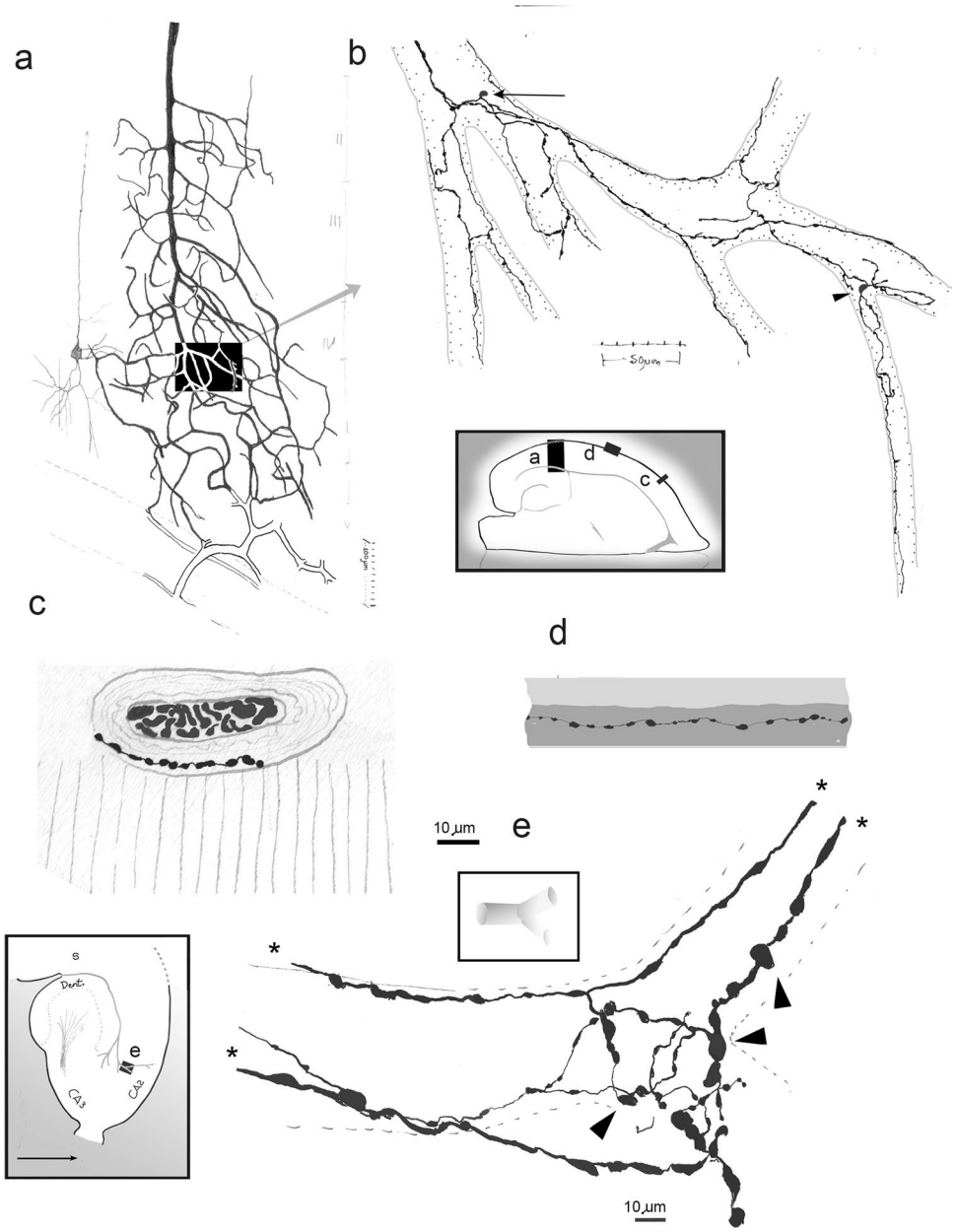


**Fig. 3** Camera lucida drawings illustrating perivascular neurons (PIN) and axonal fibro-vesicular complexes in the cerebral cortex. **a** Survey view of a long cortical blood vessel, tributary branches, and deep cortical veins (outlined in soft pencil) in the adult rat parietal cortex. Cortical layers are designated with Roman numerals in soft pencil. **b** Higher magnification image of the area boxed in **a**. Pattern of ramification and distribution of a pseudomonopolar (arrow) and a bipolar (arrowhead) PINs and their processes within the deep cortical blood vessels (soft pencil). Note the distribution of fibro-vesicular complexes associated with the blood vessel ramifications, and that thinner fibrils persist in small caliber blood vessels. Images of the rat parietal cortex are shown. **c** Arteriole at the brain surface (vertical lines in soft pencil). Note the putative motor axon located in the media layer embedded in smooth muscle fibers. **d** Longitudinal section through a meningeal arteriole with a putative motor ending distributed in the muscular wall (deep gray). Intima = pale gray. **e** Horizontal section through a penetrating blood vessel proceeding between the rabbit subiculum (s) and dentate gyrus (dent.) to distribute in the hippocampus (i.e., CA2 and CA3 = Ammon's horn, sectors 2 and 3) (inset). A fibro-vesicular complex arises from the passage of twin nerve fibers (asterisks) around the site of a vascular ramification (dashed). Note the thin fibers alternating with bulb-like enlargements of assorted diameters (arrowheads). **c**–**e** Images of the rabbit hippocampus processed with Rapid-Golgi technique

(see Kruger et al. 2003 and; Bewick 2015). Hence, we expected that primary antibodies directed against CGRP or VGlut 1, which are present in sensory fiber-terminal and mechanoreceptors (Uddman et al. 1985; Ishida-Yamamoto et al. 1988; Silverman and Kruger 1990; Álvarez et al. 1993; Johansson et al. 1999; Fujiyama et al. 2001; Nakajima et al.

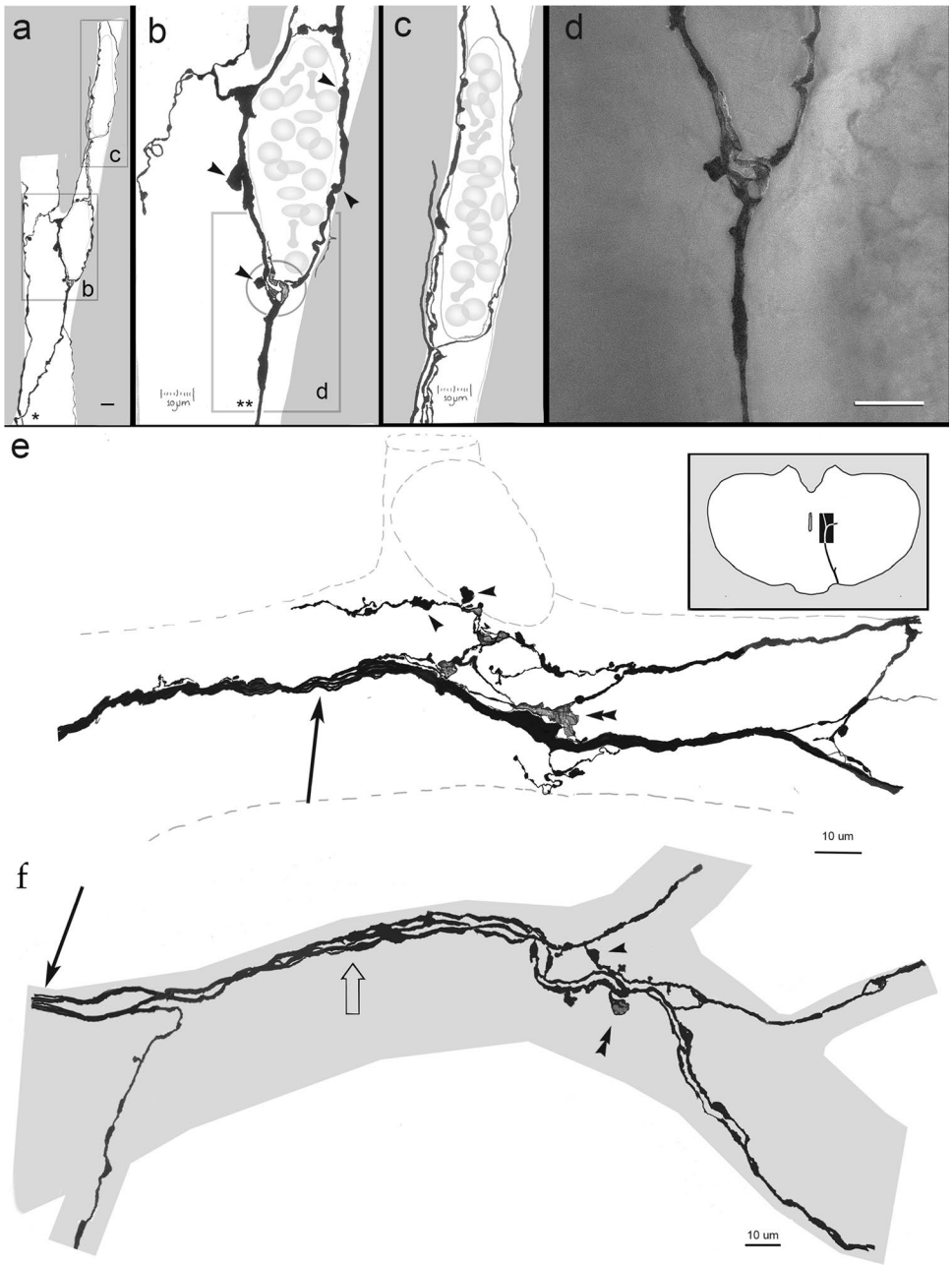


**Fig. 4** Images depicting the distribution of fibro-vesicular complexes associated with ramifying blood vessels impregnated with the Golgi technique. **a** Progression of twin nerves (asterisk) forming fibro-vesicular complexes at sites of blood vessel ramifications. **b** High-magnification image of the area outlined in **a**. Ramification of a parent fiber (double asterisks) forming series of alternating flat vesicles (encircled) and bulb-like (arrowheads) structures. **c** High-magnification image of the squared area outlined in **a**, showing another fibro-vesicular complex. **d** Photomontage of the area outlined in **b**. Images from the rat hippocampus in **a**–**d. e** Fibro-vesicular complex associated with a trifurcating blood vessel (dashed outline). Note the fasciculation of the parent fiber (arrow) prior to the formation of a fibro-vesicular complex. Arrowheads = bulbs; double arrowheads = flat, vesicular outgrowths. **f** Fasciculated fibers (arrow) forming a fibro-vesicular complex. Arrowhead = bulb-like; double arrowhead = flat, membranous outgrowth. Images of the adult rat brain in **a**–**d** and of the adult rabbit brain in **e** and **f**

2007; Lennerz et al. 2008; Mazone and McGovern 2008; Bewick et al. 2015), as well as IB4 histochemistry, should reveal putative PIN–FVCs.

The present study emphasizes immunoreactive structures associated with central blood vessels. Horseshoe and annular structures surrounding putative arteries and capillaries were visualized in specimens immunostained for antibodies to CGRP and VGlut1 and specimens subjected to IB4 histochemistry (Fig. 5a, b). In brain sections from a transgenic mouse line expressing eGFP under the control of GFAP promoter (see Varela-Echavarría 2017), astrocytic EF outline and co-fluoresce with CGRP and IB4 creating perivascular annuli. High-magnification views (Fig. 5c) reveal small clusters positive for IB4 that colocalize and overlap with areas of CGRP and VGlut1 colabeling (Fig. 5b, c). Since nitric oxide-positive neurons have been implicated in mechanosensory transduction (vide supra) and in influencing functional hyperemia (see Idecola and Nedergaard 2007), immunohistochemistry and histochemistry were performed separately to visualize nitrergic neurons and their processes. Presumptive PINs located in the capillary mesangium display strong cytoplasmic positivity to the nitric oxide synthesizing enzyme (i.e., NADPH) (Fig. 5d). Histochemical staining for nNOS reveled thin, varicose fibrils that outlined

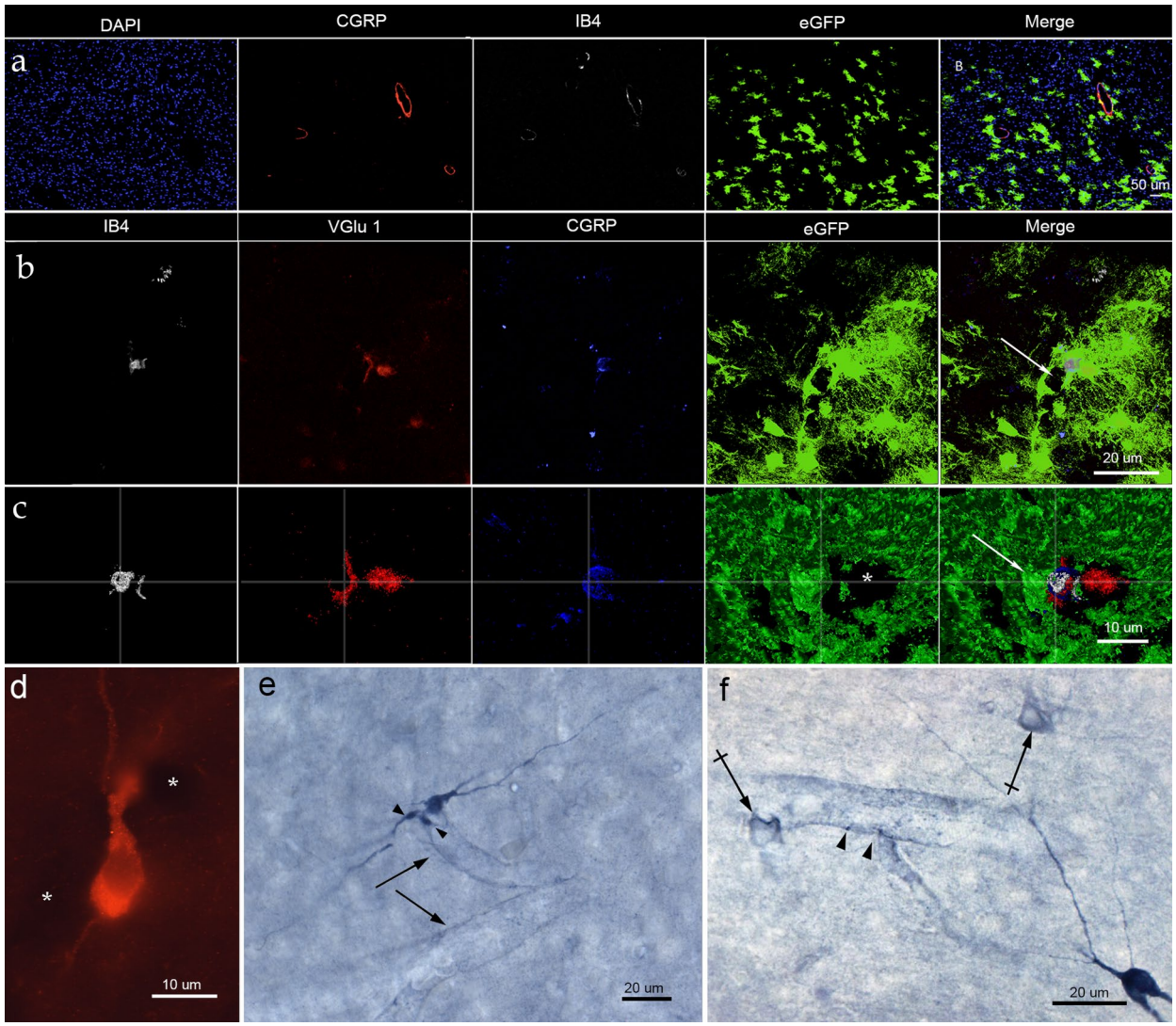


**Fig. 5** Fluorescence and confocal microscopy images of structures associated with central blood vessels. **a** Survey view of the posterior thalamic area. Note the CGRP and IB4 fluorescence in donut-like structures outlining immuno-negative blood vessels with focal overlapping with eGFP expressed in presumptive astrocytic end-feet. **b** Note the overlapping focal reactivity of IB4, with CGRP, and eGFP fluorescence alongside the lumen of a presumptive blood vessel (arrow). Images of the parietal cortex. **c** Immunofluorescence staining showing a putative perivascular bulb encased by an end-foot (arrow) next to a blood vessel (asterisk). Images were obtained with Amira software of the frontal cortex **d** a perivascular nNOS-positive neuron bounded by two blood vessels (asterisks). **e** Neurons and processes associated with blood vessels. Notice the small, rounded, structures (arrowheads) beside a neuron displaying strongly positivity to the NADPH reaction. Blood vessels appear to be outlined by thin, faintly positive, fibrils (arrows). **f** Ring-shaped processes (crossed arrows) and puncta (arrowheads) outlining the blood vessel wall. Images of the parietal cortex are shown in **d**–**f**

and encircled blood vessels (Fig. 5e, f). Perivascular cells sharing somatic and dendritic morphology with PINs were immuno-positive in specimens for GABA, NPY, and somatostatin (Online Resource, Fig. 2c–e), but negative to calbindin (see Suárez-Solá et al. 2009).

## Electron microscopy

As the fine structures of central neural and glial elements associated with the vascular wall have been extensively analyzed elsewhere (Maynard et al. 1957; Jones 1970; Peters et al. 1976; McDonald 1983; Hamel 2004; Whitman et al. 2010) our description focuses on the blood vessel wall in specimens from the frontal and parietal isocortices, posterior thalamus, and olfactory bulb medulla. Due to the superior fixation achieved in the rat specimens, 3D reconstructions were performed using this species.

PINs. Survey views of the putative PIN perikaryon reveals its slender, cigar-shaped contour (Fig. 6a, g). The scarce cytoplasm averaging a 2:10 cytoplasm/nucleus ratio

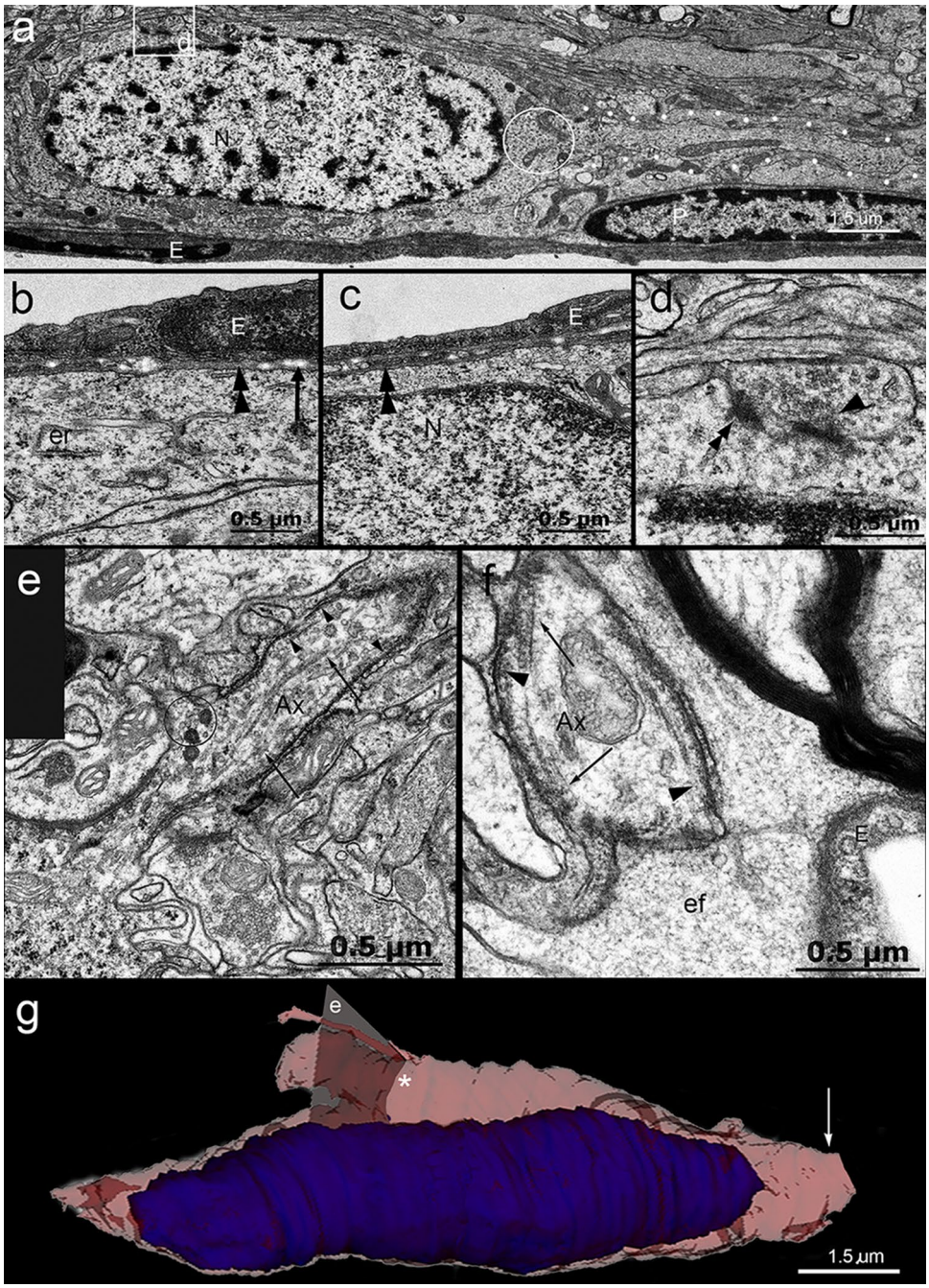


**Fig. 6** Inner and outer structures of the soma and proximal processes of perivascular neurons in the cerebral cortex. **a** Bipolar, possibly, spindle-shaped neuron paralleling a capillary blood vessel. The neuronal cytoplasm is scarce, containing numerous free ribosomes and scattered mitochondria (circle). A solitary thick dendrite (dots) courses horizontally. *E* endothelial cell, *P* pericyte. **b** Direct interaction of the dendrite (center) from a perivascular hippocampal neuron. The process lies in direct apposition to the basal lamina (double arrowhead) in which collagen fibrils (arrow) are embedded. *er* endoplasmic reticulum. **c** Perikaryon of a perivascular neuron in contact with the capillary basal lamina (double arrowhead) surrounding the overlaying endothelium (E). *N* cell nucleus. **d** Asymmetrical, axo-somatic synapse of the neuron shown in **a**. Note the numerous rounded vesicles (arrowhead) polarized towards the synaptic active zone (double arrowhead). **e** Axon initial segment of a perivascular neuron. The axon arises from the soma (bottom left side) and contains small bundles of neurotubules (arrows) and assorted vesicles (circle). Note the fuzzy, electron-opaque material (arrowheads) beneath the axon (Ax) plasma membrane. **f** Unmyelinated axon (Ax) from a perivascular neuron encased by an astrocytic end-foot (ef) next to a capillary blood vessel. *E* endothelial cell cytoplasm. Arrows = neurotubules, arrowheads = submembrane electron-dense material. **g** Reconstruction of the perivascular neuron perikaryon. Note the scarce cytoplasm (pink) surrounding the cell nucleus (blue), the side view of the axon initial segment shown in **e** (asterisk), and the root (arrow) of a dendrite. A series of two hundred and twenty sections was assembled with the Reconstruction software

contains poorly differentiated organelles, including abundant free ribosomes and scattered mitochondria; cisterns of the rough endoplasmic reticulum are indistinct (Fig. 6a, b). A solitary dendrite coursing parallel to the capillary wall is commonly observed. In 3D reconstructions of two neurons in the cerebral cortex, the origin of the axon was completely visualized. In one reconstruction, the axon arises from the lateral surface of the perikaryon (Fig. 6 e, g) and in the other (not shown), it arises from the cell pole opposite to the dendritic process. As described in a previous study for neurons of the oval nucleus of the bed nuclei of the stria terminals (Larriva-Sahd 2006), the initial segment of the axon contains clusters of small, clear- and dense-cored-vesicles, both of which are entangled by neurotubules. The bounding plasma membrane of both the initial segment (Fig. 6e) and the distal axon (Fig. 6f) are underscored by a stripe of fuzzy, electron-dense material. The cell body and proximal processes are surrounded by the capillary basal lamina and neighboring neuropil, whereas the axon courses underneath or is surrounded by EF (Fig. 6f). One or two synaptic boutons define asymmetrical contacts with the PIN perikaryon (Fig. 6a, d) and resemble those described by Blasko et al. (2013) for nNOS-positive neurons in the rostral migratory stream.

Observations of the perivascular and mesangial neuropil reveal the presence of groups of bulb-like structures with similar sizes, shapes, and locations (Figs. 7, 8, 9 and 10) to the FVCs as observed under the photic and fluorescent light microscopes. Clusters of two–five PVBs are organized and located between the capillary endothelium (McDonald 1983; Bruns and Palade 1968; Jones 1970; Peters et al. 1976) and the surrounding neuropil. PVBs are located in apposition to-, or embedded in the endothelial and pericyte capillary basal laminae and, EF (Figs. 7a, b and 8a, d, f, and g), and are in focal contact with Mato cells (Mato et al. 1984) (not shown). Observations of a series of up to 150 sections reveal that each PVB derives from an unmyelinated axon, as suggested by observations of single sections (Fig. 6e, f). Figures 7a, c, d, and 10 show a narrow proximal axon that enlarges abruptly to the PVB itself, which narrows in the opposite pole to form a distal axon, with the same inner structure as the former. Terminal PVBs arising from a stem axon, although infrequent, are revealed by 3D reconstructions (Fig. 10c).

The PVB itself contains assorted membranous organelles entangled by small bundles of neurotubules. The organelles include numerous, laminated secretory granules, mitochondria and multivesicular bodies, in decreasing frequency (Fig. 8). SGs contain concentric membranes embedded in an electron-dense matrix and although generally rounded, the presence of flat, elliptical, or pleiomorphic shapes is nonetheless common (Fig. 8). Frequent fusion of SGs with the limiting plasma membrane and occasional reinforcement of its outer aspect is observed (Fig. 8b, between arrows, c). Overall, the organelles described here for the PVB, particularly its secretory granules, recapitulate the organelles observed in the Meissner corpuscle from the same animal (Online resource Fig. 5) (Hashimoto 1973; Ide et al. 1987), as well as the sensory endings of the Pacinian corpuscle and other peripheral sensory receptors (Chouchkov 1973; Kimani 1992; Malinovsky 1996; Maeda et al. 1999; Iigima and Zhang 2002; Kruger et al. 2003).

Another specialization that is approximately one-third of PVBs in the neocortex, hippocampus, and posterior thalamus, consists of typical asymmetrical synapses (Figs. 8f, 9a–c) (Peters et al. 1976). These PVB synapses consist of collections of small, rounded synaptic-like vesicles (SLVs) with electron-lucid matrices that converge onto a synaptic contact shared with a dendritic spine. Small membranous collections are commonly observed within the cytoplasm of the dendritic spine (Fig. 8g). An interaction between astrocytic EF and the PVB synapse (Fig. 9a–c) is commonly observed. In 3D reconstructions, SLVs are polarized towards the synaptic active zone, whereas secretory granules are distributed throughout the PVB cytoplasm (Fig. 9d, e).

PVBs are housed in a complex framework formed by the elements of the NVU. Both the PVB and its parent axons are enveloped by an elaborate cuff composed of the capillary basal laminae and astrocytic EF in varying proportions (Figs. 9a–c, 10). An exception for this is noted in capillaries of the olfactory bulb medulla, whose neuronal precursors and their processes envelop a substantial part of the PVB surface (Fig. 7a, b). Additionally, PVBs are invariably embedded in the basal lamina, which organizes an amorphous receptacle of varying thickness. Focal areas devoid of the basal membrane enclosure are covered by EF, thereby completely encasing the PVBs. In addition to the glial–basal laminae interaction, the surface of a small subset of PVBs observed in the olfactory bulb and cerebral cortex is directly exposed to the neighboring neuropil (see above) (Fig. 8a).

## Discussion

### Perivascular interneuron or ganglion cell?

We describe a unique group of perivascular interneurons or PINs intrinsic to the NVU of the vasculature in the adult brain and brainstem. PINs are identified in a lissencephalic (i.e., rat) and three gyrencephalic (i.e., rabbit, cat, and monkey) species, hence, highly conserved in mammals. Based on its outstanding distribution and interactions with the NVU, the PINs should be considered a new cell type. Overall, is the PIN's soma and its processes are confined to the perivascular domain and frequently surrounded by the capillary basal laminae and astrocytic EF. The PIN described here appears to correspond to a

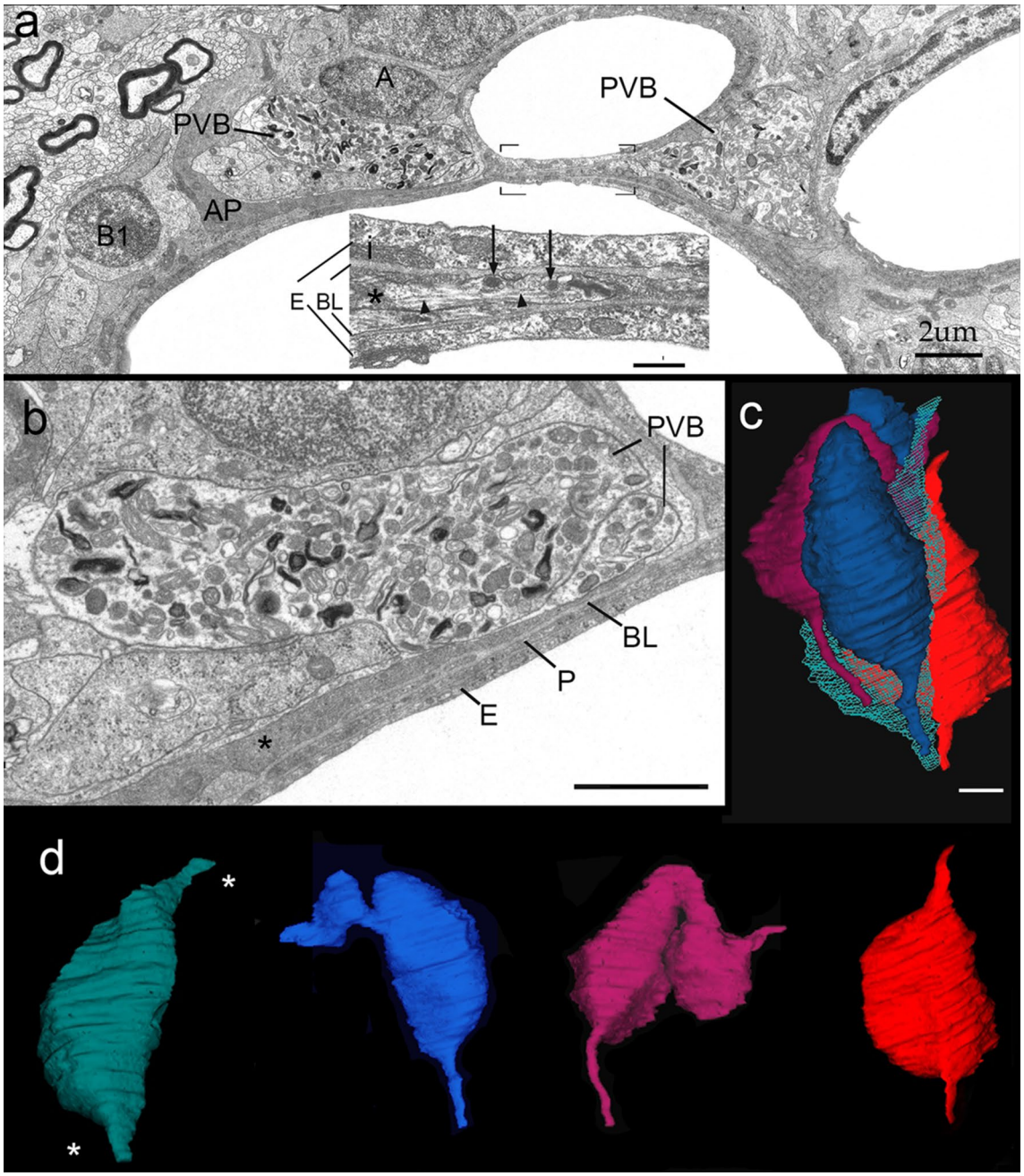


**Fig. 7** Two- and 3-dimensional electron microscopy images of clusters of perivascular bulbs (PVBs) contiguous to a presumptive vascular trifurcation within the rat olfactory bulb medulla. **a** Survey micrograph showing the interactions of PVBs with capillary basal laminae, astrocytic processes (AP), and a presumptive adult-born cell-precursors (A and B1) (Doetsch et al. 1997). i High-magnification image depicting an axon (asterisk) arising from a PVB passing between the two capillary basal laminae (BL) beneath endothelial cells (E). The PVB axon contains dense-cored vesicles (arrows) and sparse microtubules (arrowheads). **b** PVBs bounded by two capillary blood vessels. The numerous mitochondria and electron-opaque membranous organelles contained by a limiting cell membrane with a smooth contour are evident. Asterisk = process of a putative A cell (see above), *E* endothelium, *P* pericyte, and *BL* basal lamina. **c** Reconstruction of a cluster of four complete PVBs contained in one-hundred and eighty-four consecutive sections. **d** Outer aspect of the bulbs shown in **c**. Note that each bulb results from the expansion of an axon that narrows at the poles (see **a**, inset); the resulting processes proceed distally from either bulbar pole (asterisks)

subset of type 1 nNOS-positive interneurons that form a dense perivascular framework and extend long processes that may contact distant arterioles and capillaries (Estrada et al. 1993; Idecola et al. 1993; Estrada and DeFelipe 1998; Suárez-Solá 2009). To the best of our knowledge, cytological information about perivascular neurons and

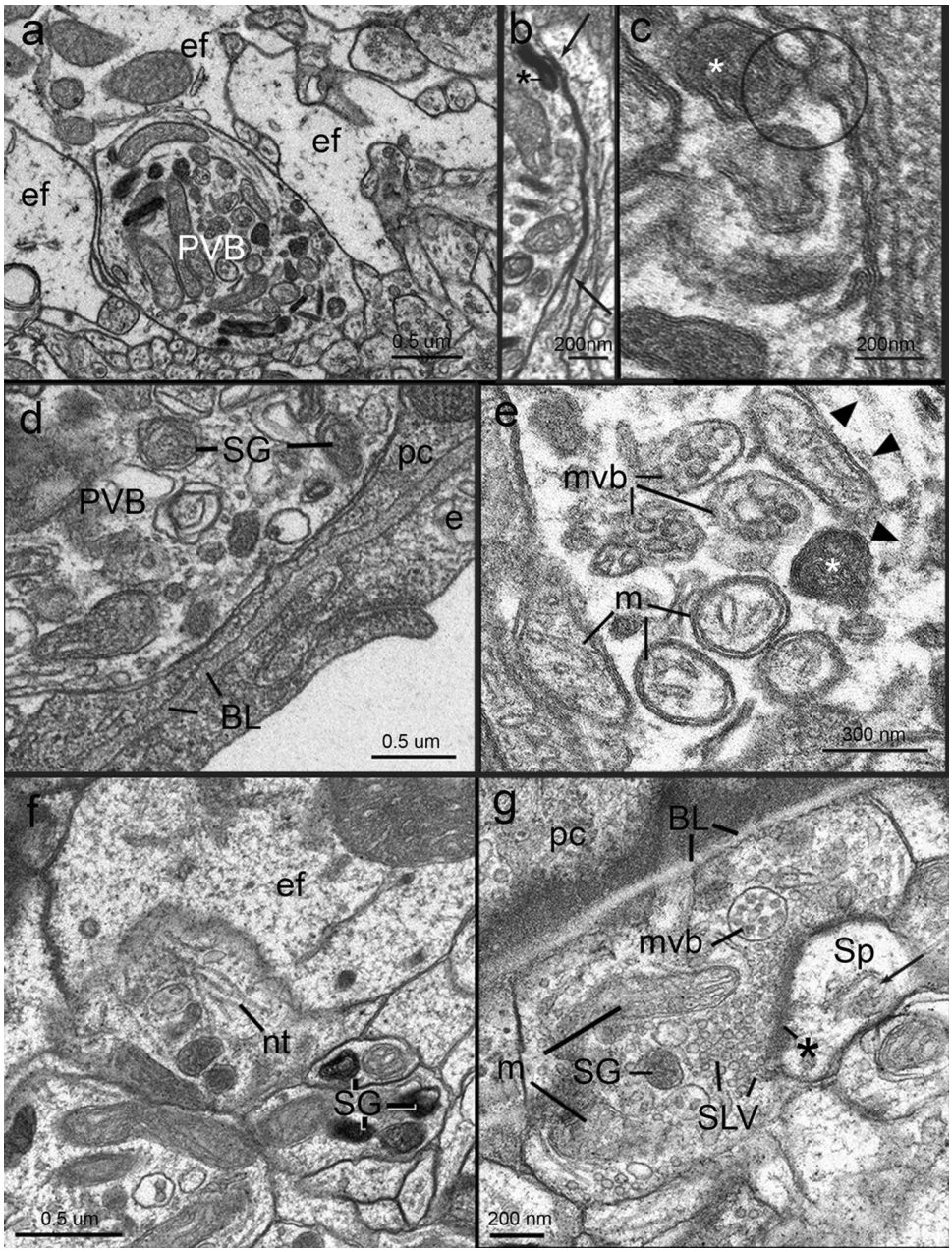


**Fig. 8** Organelles and interactions of perivascular bulbs (PVB) within the neurovascular unit of the adult rat. **a** A PVB partially encased by astrocytic end-feet (ef) and neuropil (bottom) that contains laminated secretory granules, mitochondria and assorted vesicles. **b** Outer aspect of a PVB outlined by a neuronal process. Notice the fusion of a laminated secretory granule (*) with the bulbar plasma membrane, which is reinforced by an electron-opaque material (between arrows). **c** Fusion of a membranous secretory granule (asterisk) with the plasma membrane (circle). **d** Relationships between a perivascular bulb (PVB) and the capillary wall. Note that the PVB faces directly a pericyte (pc). *BL* basal lamina, *e* endothelial cell. **c**–**d** Images of the posterior thalamus. **e** High-magnification micrograph of PVB-containing multivesicular bodies (mvb) bounded by mitochondria with vesicular cristae (m), neurotubules (arrowheads), and a laminated secretory granule (asterisk). **e** Image of the frontal cortex. **f** Cluster of PVB, one of which faces end-feet (ef). *SG* laminated secretory granules, *nt* neurotubules. **g** A PVBs partially covered by the basal lamina (BL) of a pericyte (pc). Note the numerous synaptic-like vesicles (SLV) clustered next to an asymmetrical synapse with a dendritic spine (Sp). Arrow = spine apparatus; asterisk = active zone; *m* mitochondria, *SG* secretory granule. **f**–**g** Images of the parietal cerebral cortex

their processes is not available. Hence, we opted for the Golgi technique that has been effective in defining most neuron types and peripheral receptors within the nervous system. The PIN's axon forms clusters of terminals, termed here PVBs, whose morphology, reactivity, and immunoreactivity match with those observed in sensory

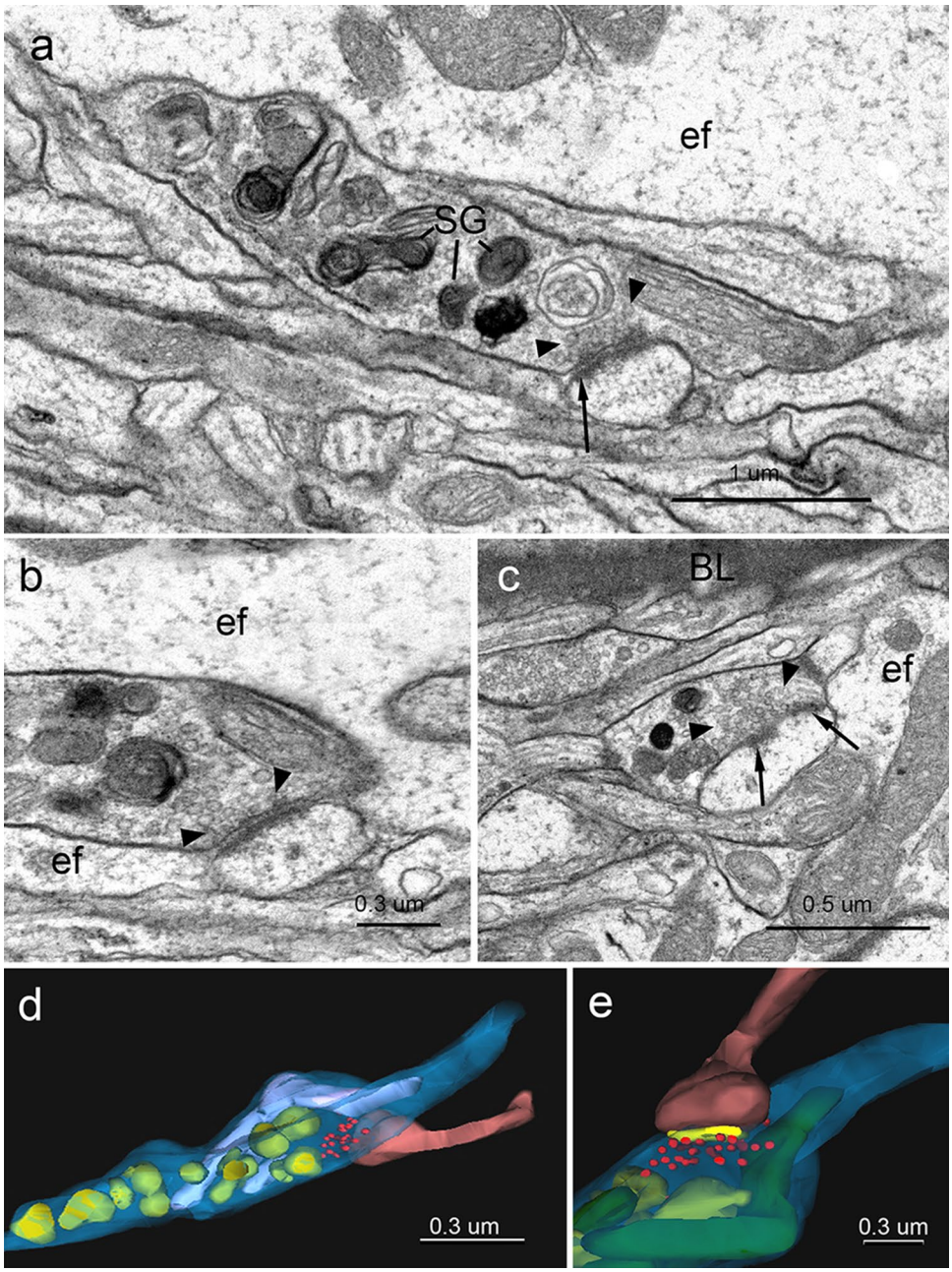


**Fig. 9** Synapses of perivascular bulbs (PVBs). **a** A perivascular bulb forms an asymmetrical synapse with a nearby spine in the underlying neuropil. Note the cluster of small clear, presynaptic vesicles next to the active zone (arrow) distributed along the pre- and postsynaptic sites in the cytoplasm. Image from the midbrain. **b** High-magnification image of a PVB forming an asymmetrical synapse encased by astrocytic end-feet, resulting in a tripartite synapse (Araque et al. 1999). An image of the frontal cortex is shown. **c** PVB forming a spinous synapse with two active zones (arrows). *BL* capillary basal lamina, *ef* end-foot. An image of the deep parietal cortex. **d** A 3D reconstruction of the perivascular bulb shown in **a**. The pale cytoplasm (turquois) harbors numerous laminated secretory granules (green), two mitochondria (light blue) and a cluster of synaptic-like vesicles (red) beneath the site of apposition with the dendritic spine (pink). **e** High-magnification of the synaptic interaction shown in **d** to which the active zone (yellow) has been added. Images generated with the Reconstruct software

axons of the Meissner corpuscle and in other peripheral mechanoreceptors. Based on cytological characteristics, the PIN may be considered a variant of the peripheral ganglion cell. In fact, like the distal branch of a ganglion cell, the PIN's axon is characterized by a presumptive sensory ending. Furthermore, glial and perivascular basal laminae observed in mechanoreceptors (Andres and During 1973; Dubvový and Bednárová 1999) encase the putative sensory ending of the PIN. Moreover, the twin fiber fasciculation and sequential distribution of the spindle-shaped PIN-FVC axon at sites of vascular ramifications might be regarded as a central form of functional segmentation (Fig. 3e–f). The early assumption of the peripheral ganglion cell as a mere relay neuron proved to be an oversimplification; it in fact receives several peripheral inputs and its central process diverges before resolving in the spinal cord (Langford and Coggeshall 1981). Hence, spatially dissimilar, segmental receptor fields recruit the same ganglion cell (Christianson et al. 2007), supporting the ability of this cell type to decode time–space sensory cues. Similarly, the axon of the spindle-shaped PIN originates a series of FVCs that distribute sequentially in the arising capillary blood vessels (Fig. 2a) thereby suggesting that spatial decoding is

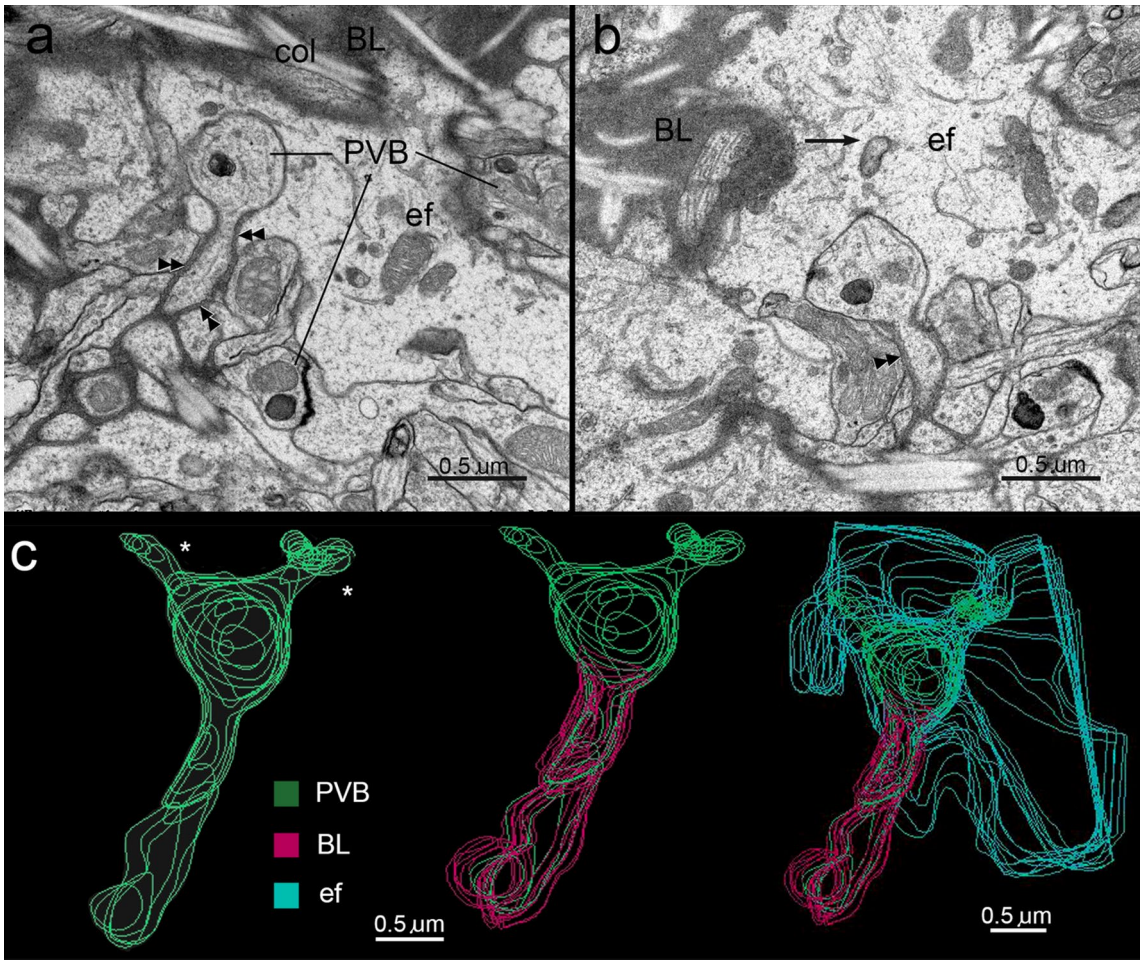


**Fig. 10** Series of electron micrographs depicting the structure and interactions of perivascular bulbs (PVBs) with the neurovascular unit. **a** Image of a tangential section through the periphery of a capillary blood vessel exhibiting three PVBs. Note that the bulb on the left is encased in astrocytic end-feet (ef), whereas the basal lamina (arrowheads) covers its stem axon. *BL* capillary basal lamina, *col* collagen bundles. **b** Specimen located fourteen sections away from the section shown in **a**. Notice that the bulb and its stem fiber remain encased by the astrocytic end-foot (ef) and basal lamina (arrowheads), respectively. Arrow = bulbar appendage. **c** Stepwise reconstruction of the bulb and its stem axon displaying the increasing encasement by the basal lamina (red) and astrocytic end-foot (turquoise). The paired bulbar appendages climbing towards the blood vessel wall (not shown). Images of the frontal cortex of the adult rabbit

mediated by the PIN itself. Because the diameter of the blood vessel decreases as it flows distally (Hall 2016), the parallel vascular distribution of the PIN and its processes should be exposed to a similarly dynamical force. Aside from the potential implications of blood flow dynamics (Fig. 11d), the axonal distribution of the PINs suggests that, like the ganglion cell, the PIN perikaryon decodes dissimilar segmental inputs (Fig. 11a, d) (see Larriva-Sahd 2014). While this hypothetical ability of the PIN to decode time–space inputs is open to future neurophysiological assessments, its striking analogy with the peripheral sensory neuron suggests that it corresponds to a ganglion-like cell. Notwithstanding the drawbacks of deducing the function from the structure alone, the novelty of this putative receptor suggests some functional correlates, as discussed below.

## Perivascular neuron connectivity

While we were unable to identify axons projecting from the PIN to the neighboring neuropil, the synaptic interactions of PVBs with typical dendritic spines (Arellano et al. 2007) provide a valuable clue to its connections. In fact, the association of synaptic-like vesicles with the neighboring glial and stromal cells in peripheral mechanoreceptors has been thoroughly investigated, and thus a consensus about their functional roles has been reached. At first glance, the presence of synaptic vesicles within the primary sensory endings was found to be paradoxical,

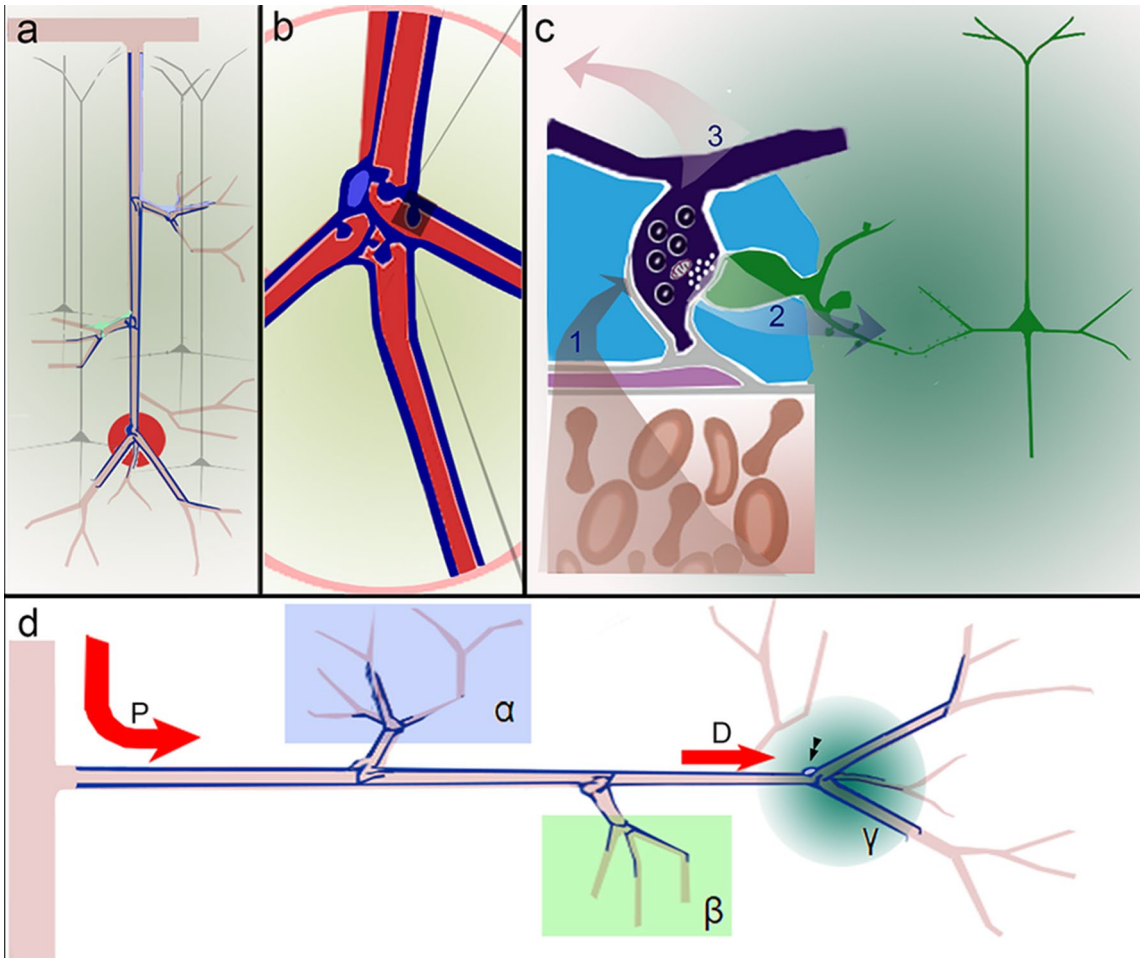


**Fig. 11** Cartoons illustrating morphological and functional correlates of perivascular interneurons (PIN), axons, and fibro-vesicular complexes (FVCs) they form. **a** A set of deep perivascular neurons (blue) extends long, ascending axons that, produce a series of fibro-vesicular specializations around the blood vessel ramification (one is encircled in red). **b** Within the neurovascular unit, each fibro-vesicular complex gives rise to numerous perivascular bulbs (one is shaded). **c** Putative feed-back mechanism controlling blood flow. Blood flow (bottom) produces a mechanical impact on the neurovascular unit, including perivascular bulbs (deep blue) (arrow 1) leading to a receptor-mediated, i.e., graded, response. Receptor-mediated potentials may travel to the cell body (vide infra) (arrow 3) or provoke neurotransmitter release to dendritic spines of nearby neurons (arrow 2). **d** Note that the sequential arrangement of FVCs from the proximal (P) to the distal (D) part of the artery may sense both local mechanical blood flow variations within each ramification and the overall blood flow within the PIN perikaryon (arrowheads). For instance, opening of the blood vessel in (α) during functional hyperemia decreases the flow in stem blood vessel (Vector D) which, may, in turn, be sensed by the PIN perikaryon and proximal processes at the "γ" territory (turquoise). Upon further blood flow demand in territory beta (β), would likewise implicitly further decrease the overall magnitude of Vector D, territory gamma (γ). If the PIN, similar to other neurons in the CNS (see Larriva-Sahd 2014), decodes temporal and spatial inputs, it would then be able to monitor both segmental blood flow (i.e., α, β, and γ) and the overall flow throughout the blood vessel

or at least atypical (see Kruger et al. 2003). Subsequent experience supported the involvement of synaptic-like vesicles in vGlut 1-mediated glutamate recycling at the mechanosensory ending-receptor interphase (Bewick and Banks 2015) further suggesting that the synaptic-like vesicle-receptor contacts are the structural signature for the sensory ending-mediated tune-up of the receptor itself (Bewick 2015). In the present study the reactivity of the putative PVB to the vGlut1 antibody further supports its receptor nature. However, a fundamental difference exists between the PVB-synapse and the contact of the primary sensory nerve–receptor interaction. Synaptic-like vesicles in sensory endings polarize towards the glial or cellular elements associated with the receptor, whereas in the PVB vesicles form the presynaptic element of typical axo-spinous synapses. Hence the PVB appear to modulate nearby neurons via chemical synapses. How do sensory cues, mechanical or otherwise, elicit receptor potentials in the PVB? Although we are unable to answer this question here, the similarities of the vascular and glial elements associated with the PVBs with those of peripheral mechanoreceptors are striking.

## Stromal and glial components of the perivascular bulb structure, a perivascular organ

Sensory endings and associated glial and stromal structures define sensory organs. The PVB and associated endothelial cells, pericytes, EF and extracellular matrix, appear to be their counterparts. What is the potential involvement of each of these structures? Endothelial cells that are continuously exposed to mechanical stimulation display complex responses to mechanical stress. Complementarily, astrocytes exert a permissive effect in modulating functional hyperemia (Attwell et al. 2010). Although endothelial cells (Davis 1995; Busse and Fleming 2003) and astrocytes (Davis 1995; Filosa et al. 2016) are necessary to trigger functional hyperemia and both display varying degrees of responses to mechanical stimuli, no evidence is available that they transduce these signals to receptor potentials. Stromal and astroglial cells, as well as the extracellular matrix, are nonetheless crucial for sensory transduction (see Nesslinger 1996; Zimmerman et al. 2014). In fact, the endothelial cell is very sensitive to the shear stress imprinted in the vascular wall, leading to the synthesis and release of potent vasoactive molecules (Busse and Flemig 2003). Notably, nitric oxide and the endothelial-derived hyperpolarizing factor (McGuire et al. 2001) are postulated to modulate arterial smooth muscle tone. Second are the astrocytic EF which organize a bounding annulus around the former and, perhaps equally important, around the PVB (Fig. 10) and its synapses (Fig. 9a, b). In fact, association of astrocytic processes enveloping both pre- and postsynaptic elements represents the structural substrate responsible for the modulatory effect of astrocytes on chemical transmission (Araque et al. 1999; Tasker et al. 2012). Since astrocytes are very responsive to blood flow demands (Idecola and Nedergaard 2007; Attwell et al. 2010; Filosa et al. 2016), we speculate that EF surrounding PVBs may in the same fashion modulate its eventual synaptic output. The identity of the PVB postsynaptic neuron is currently being investigated in an ongoing ultrastructural 3D study. An emerging corollary is that the PVB-spine synapse is a functional link between this putative receptor and the neural circuitry involved in sensory decoding for an appropriate vasomotor response.

## Sensory innervation of the brain vasculature: functional implications

Functional brain parcellation is based upon variations in functional hyperemia elicited by cellular energy demands. Notably, functional magnetic resonance imaging, near infrared spectroscopy, and other noninvasive procedures take advantage of the dynamic, differential blood flow to define the functional recruitment of discrete territories of the brain. (see Idecola 2004; Filosa et al. 2016). While the cardiac output is constantly monitored by specialized sensory organs in the systemic circulation, researchers do not clearly understand how changes in blood flow during functional hyperemia feed-back to regulate vasomotor responses. The PINs described here represents an attractive candidate that should be further explored. In fact, the utilization of in vivo recordings combined with pharmacological tools should help in defining the physiological roles of the neurochemicals identified here in association with PVBs.

Given the paramount roles of blood vessels and the blood supply in metabolism, nourishment, development, and normal and pathological plasticity in the brain, a systematical review of all potential effects of mechanoreception, should be left as an open chapter (see Ward and Lemana 2004; Idecola 2004). However, the association of PVBs with cells and their processes that are phenotypically indistinguishable from those of adult-born neuron precursors observed in the olfactory bulb medulla (Doetsch et al. 1997) (Fig. 7a, b), prompt some remarks. The OB is one of the privileged brain areas of the adult brain, in which newborn neurons migrate from the lateral ventricle to the bulbar cortex where they incorporate into preexisting circuits. Blood vessels and glial cells are intimately implicated in the viability, induction, and guidance of prospective adult-born neurons (Whitman et al. 2010). Notably, blood vessels (Whitman et al. 2010), extracellular matrix (Hallmann et al. 2005), and astroglia (Lois and Alvarez-Buylla 1994) guide differentiating neurons to their eventual targets, a process involving numerous signaling and trophic molecules expressed and/or released by and within by the NVU itself (Ward and Lemana 2004). How do prospective neurons recognize the source and the target for a successful journey? In effect, a blood vessel, i.e., a cylinder, lacks the required polarity to modulate the sequential expression and/or secretion of signaling molecules and trophic factors by the NVU itself. One possibility is that the putative receptor described here transduces directionality, which is generated by the functional hyperemia, to the former (Fig. 11d). A tempting speculation is that the PIN and its stromal and glial partners would, directly or indirectly instruct neuronal precursors about eventual site(s) where they are required to meet the increased metabolic demands (Sharp et al. 1975; Magavi et al. 2005; Alonso et al. 2008). In fact, functionally recruited glomeruli trigger functional hyperemia (see Xu et al. 2000; Chaigneau et al. 2003; Alonso et al. 2008) such that blood flow from tributary blood vessels is redirected to the former. Because of the negligible elasticity of the blood column, a functional sink is created. Our observations in Golgi-impregnated specimens show that blood vessels in the core of the olfactory bulb ascend radially to the olfactory cortex, resolving into glomerular veins and venous sinuses (Online resource Fig. 6); accordingly, functional hyperemia within a given

glomerulus should modify blood flow in a retrograde manner. Although arterial and venous blood vessels may be readily identified with the Golgi technique (see above and Marin-Padilla 2012), the blood flow direction is unable to be defined in a histological section. However, this limitation does not challenge the essence of our hypothesis that the blood flows towards (See Lecoq et al. 2009) or away from a glomerulus retrogradely or anterogradely affects blood flow variations (Hall 2016), respectively. We therefore postulated that the decoding of blood flow variations by series of PVBs (Fig. 11d) would enable the NVU to influence the migratory processes of prospective neurons progressively towards functionally active territories.

## Concluding remarks

The FVC–PVB recapitulates the neural, glial, and stromal elements observed in some peripheral mechanoreceptors for which a likewise sensory function is suggested for the former.

Edgar Adrian (1954) described the physiological characteristics of mechanoreceptors and determined that the stretching of tendinous sensory endings (Sherrington 1892) results in receptor potentials whose frequency varies as a function of the intensity of the stimulus. This remarkable property of receptors was soon extended and found to exist in all sensory organs and terminals. In the systemic blood flow, receptor organs and endings are strategically positioned to sense and transduce physical and chemical cues that are decoded by the CNS to drive appropriate motor responses in the heart, blood vessels, and endocrine system (Hall 2016). The structural identification of a putative mechanoreceptor in precapillary and capillary blood vessels within the CNS suggests that like the systemic blood circulation, subtle hydrodynamic variations in distal blood flow are likewise transduced to neuron chains for a successful adaptative motor outcome. The associations of PIN–FVCs with the NVU as a counterpart of the peripheral ganglion cell-receptor support the existence of brain proprioception (i.e., self-sensorial).

**Acknowledgements** This work was supported by CONACyT, Grant 1782 to LC and JL-S and by Universidad Nacional Autónoma de México, PAPIIT Grant IG200117 to LC and JL-S. The transgenic hGFAP-GFP mouse line was a generous gift from Dr. Helmut Kettenmann. Authors appreciate the numerous suggestions made from Dr. Carlos Cepeda on our manuscript and thank Gema Martínez-Cabrera, Carlos Lozano-Flores Flores, Lourdes Palma, Elsa Nydia Hernández-Ríos, Martín García, and Rafael Olivares for providing technical assistance. The thorough revision of our manuscript by Jessica González Norris and American Journal Experts is also appreciated.

## References

Adrian ED (1954) The basis of sensation. Br Med J 1:287–290
Alonso M, Ortega-Pérez I, Grubb MS, Bourgeois J-P, Charneau P, Lledo P-M (2008) Turning astrocytes from the rostral migratory stream into neurons: a role for the olfactory sensory organ. J Neurosci 28:11089–11102
Alvarez FJ, Kavokjian AM, Light AR (1993) Ultrastructural morphology, synaptic relationships, and CGRP immunoreactivity of physiologically identified C-fiber terminals in the monkey spinal cord. J Comp Neurol 329:472–490
Andres KH, von During M (1973) Morphology of cutaneous receptors. In: Iggo A (ed) Handbook of sensory physiology. vol. II. Somatosensory system. Springer, Berlin, pp 3–28
Araque A, Puroura V, Sanzigri RP, Haydon PG (1999) Tripartie synapses: glia, the unacknowledged partner. Trends Neurosci 22:208–215
Arellano JI, Benavides-Piccione R, De Felipe J, Yuste R (2007) Ultrastructure of dendritic spines: correlation between synaptic and spine morphologies. Front Neurosci 15:131–143. https://doi.org/10.3389/neuro.01.1.1.010.2007
Attwell D, Buchan AM, Charpak S, Lauritzen M, Macvicar BA, Newman EA (2010) Glial and neuronal control of blood flow. Nature 468:232–243
Barone P, Kennedy H (2000) Non-uniformity of neocortex, areal heterogeneity of NADPH-diaphorase reactive neurons in adult macaque monkeys. Cereb Cortex 10:160–174
Bewick GS (2015) Synaptic-like vesicles and candidate transduction channels in mechanosensory terminals. J Anat 227:194–213
Bewick GS, Blacks RW (2015) Mechanotransduction in the muscle spindle. Eur J Physiol 467:175–190
Blasko J, Fabianova K, Martocikova M, Sopkova D, Racekova E (2013) Immunohistochemical evidence for the presence of synaptic connections of nitrergic neurons in the rostral migratory stream. Cell Mol Neurobiol 33:753–757
Bruns RR, Palade GE (1968) Studies on blood capillaries. I. General organization of blood capillaries in muscle. J Cell Biol 37:244–273
Busse R, Fleming I (2003) Regulation of endothelium-derived vasoactive autacoid production by hemodynamic forces. Trends Pharmacol Sci 24:24–29
Cauli B, Tong XK, Rancillac A, Serluca N, Lambolez B, Rossier J, Hamel E (2004) Cortical GABA interneurons in neurovascular coupling: relays for subcortical vasoactive pathways. J Neurosci 24:8940–8949
Chaigneau E, Oheim M, Audinat E, Charpak S (2003) Two-photon imaging of capillary blood flow in olfactory bulb glomeruli. PNAS 100:13081–13086
Chouchkov Ch N (1973) The fine structure of small encapsulated receptors in human digital glabrous skin. J Anat 114:25–33
Christianson JA, Liang R, Ustinova EE, Davis BM, Fraser MO, Pezzone MA (2007) Convergence of bladder and colon sensory innervation occurs at the primary afferent level. Pain 128:235–243
Cohen Z, Molinatti G, Hamel E (1997) Astroglial and vascular interactions of noradrenaline terminals in the rat cerebral cortex. J Cerebral Blood Flow Metab 17:894–904
Cubelos B, Giménez C, Zafra F (2005) Localization of the GLYT1 glycine transporter and glutamatergic synapses in the rat brain. Cereb Cortex 15:448–459. https://doi.org/10.1093/cercor/bhh 147
Davis PF (1995) Flow-mediated endothelial mechanotransduction. Physiol Rev 75:519–560
Doetsch F, García-Verdugo JM, Alvarrez-Buylla A (1997) Cellular composition and three-dimensional organization of the subventricular germinal zone in the adult mammalian brain. J Neurosci 17:5046–5061

Dubvový P, Bednárová J (1999) The extracellular matrix of rat Pacinini corpuscles: an analysis of its fine structure. Anat Embryol 200:615–623

Ducheim S, Boily M, Sadekova N, Girouard H (2012) The complex contribution of NOS interneurons in the physiology of cerebrovascular regulation. Front Neural Circuits 6:1–19. https://doi.org/10.3389/fncir.2012.0005

Eftekhari S, Evinsson L (2011) Calcitonin gene-related peptide (CGRP) and its receptor components in human and rat spinal trigeminal nucleus and spinal cord t C1-level. BMC Neurosci 12:112–132

Estrada C, DeFelipe J (1998) Nitric oxide-producing neurons in the neocortex: morphological and functional relationship with intraparenchymal microvasculature. Cereb Cortex 8:193–203

Estrada C, Mengual E, González C (1993) Local NADPH-diaphorase neurons innervate pial arteries and lie close or project to intracerebral blood vessels: a possible role for nitric oxide in the regulation of cerebral blood flow. J Cereb Blood Flow Metab 13:978–984

Filosa JA, Morrison HW, Iddings JA, Du W, Kim KJ (2016) Beyond neurovascular coupling, role of astrocytes in the regulation of vascular tone. Neurosci 323:96–109

Fujiyama F, Furuta T, Kaneko T (2001) Immunocytochemical localization of candidates for vesicular glutamate transporters in the rat cerebral cortex. J Comp Neurol 435:379–387

Hall JE (2016) Textbook of medical physiology. Elsevier, Amsterdam

Hallman R, Horn N, Selg M, Wendler O, Pausch F, Sorokin LM (2005) Expression and function of laminins in the embryonic and mature vasculature. Physiol Rev 85:979–1000. https://doi.org/10.1152/physrev.00014.2004

Hamel E (2004) Cholinergic modulation of the cortical microvascular bed. Prog Brain Res 145:171–178

Hartman BK, Zide D, Undenfriend S (1972) The use of b-hydroxylase as a marker for the central noradrenergic nervous system in the rat brain. Proc Natl Acad Sci 69:2722–2726

Hashimoto K (1973) Fine structure of Meissner corpuscle of human palmar skin. J Investig Dermatol 60:20–28

Ide C, Nitatori T, Munger BL (1987) The cytology of human Pacinian corpuscles: evidence for srpouting of the central axon. Arch Histol Jpn 50:363–383

Idecola C (2004) Neurovascular regulation in the normal brain and in Alzheimer's disease. Nat Neurosci 5:347–360

Idecola C, Beitz A, Renno W, Xu X, Mayer B, Zhang F (1993) Nitric oxide synthase-containing neural processes on large cerebral arteries and cerebral microvessels. Brain Res 606:148–155

Idecola and Nedergaard (2007) Glial regulation of the cerebral microvasculature. Nat Neurosci 10:1369–1376

Iigima T, Zhang J-Q (2002) Three-dimensional wall structure and innervation of dental pulp blood vessels. Microsc Res Tech 56:32–41

Ishida-Yamamoto A, Seneba E, Tohyama M (1988) Calcitonin gene-related peptide and substance P-immunoreactive nerve fibers in Meissner's corpuscles of rats: an immunohistochemical analysis. Brain Res 453:362–366

Johansson O, Fantini F, Hu H (1999) Neuronal structural proteins, transmitters, transmitter enzymes and neuropeptides in human Meissner's corpuscles: a reappraisal using immunohistochemistry. Arch Dermatol Res 291:419–424

Jones EG (1970) On the mode of entry of blood vessels into the cerebral cortex. J Anat 106:507–520

Kimani JK (1992) Electron microscopic structure and innervation of the carotid baroreceptor region in the Rock Hyrax (Procavia capenensis). J Morphol 212:201–211

Kruger L, Light AR, Schweizer FE (2003) Axonal terminals of sensory neurons and their morphological diversity. J Neurocytol 32:205–216

Langford LA, Coggeshall RE (1981) Branching of sensory axons in the peripheral nerve of the rat. J Comp Neurol 203:745–750

Larriva-Sahd J (2006) A histological and cytological study of the bed nuclei of the stria terminalis of the adult rat. II Oval nucleus: extrinsic inputs, cell types, and neuronal modules. J Comp Neurol 497:772–807

Larriva-Sahd J (2008) The accessory olfactory bulb in the adult rat: a cytological study of its cell types, neuropil, neuronal modules, and interactions with the main olfactory system. J Comp Neurol 510:309–350. https://doi.org/10.1002/cne.21790

Larriva-Sahd J (2014) Some predictions of Rafael Lorente de Nó, eighty years later. Front Neuroanat 8:147. https://doi.org/10.3389/fnana.2014.00147. **(eCollection 2014. Review. PMID: 25520630)**

Lecoq J, Tiret P, Najac M, Shepherd GM, Greer CA, Charpak S (2009) Ordor-evoked oxygen consumption by action potential and synaptic transmission in the olfactory bulb. J Neurosci 29:1424–1433

Lennerz J, Rühle V, Ceppa EP, Neuhuber WL, Bunnett NW, Grady EF, Messlinger K (2008) Calcitonin receptor-like receptor (CLR), receptor activity-modifying protein 1 (RAMP1), and calcitonin gene related peptide (CGRP) immunoreactivity in the rat trigeminovascular system: differences between peripheral and central CGRP receptor distribution. J Comp Neurol 507:1277–1299

Lois C, Alvarez-Buylla A (1994) Long-distance neuronal migration in the adult mammalian brain. Science 264:1145–1148

Maeda T, Ochi K, Nakamura-Oshima K, Youn SH, Wakisaka S (1999) The Ruffini ending as the primary mechanoreceptor in the periodontal ligament: its morphology, cytochemical features, regeneration, and development. Crit Rev Oral Biol Med 10–307. https://doi.org/10.1177/10454411990100030401

Magavi SSP, Mitchell BD, Szentirmai O, Carter BS, Mackilis (2005) Adult-born and preexisting olfactory granule neurons undergo distinct experience-dependent modifications of their olfactory responses in vivo. J Neurosci 25:10729–10739

Malinovsky L (1996) Sensory nerve formations in the skin and their classification. Microsc Res Tech 34:283–301

Marin-Padilla M (2012) The human brain intracerebral microvascular system: development and structure. Front Neuroanat 6:1–14. https://doi.org/10.3389/fnana.2012.00038

Mato M, Ookawara S, Sugamata M, Aikawa E (1984) Evidence for the possible function of the fluorescent granular perithelial cells in brain scavenger of high-molecular weight products. Experientia 40:399–402

Maynard EA, Schultz RL, Pease DC (1957) Electron microscopy of the vascular bed of rat cerebral cortex. Am J Anat 409–433 https://doi.org/10.1002/aja.1001000306

Mazone SB, McGovern a (2008) Immunohistochemical characterization of nodose cough receptor neurons projecting to the trachea of guinea pigs. Cough 4:9–16. https://doi.org/10.1186/1745-9974-4-9

McDonald DM (1983) A morphometric analysis of blood vessels and perivascular nerves in the rat carotid body. J Neurocytol 12:155–199

McGuire JJ et al (2001) Endothelium-derived relaxing factors: a focus on endothelium-derived hyperpolarizing factor(s). Can J Physiol Pharmacol 79:443–470

Nakajima T, Ohtori S, Inoue G, Koshi T, Yamamoto S, Nakamura J, Takahashi K, Harada Y (2007) The characteristics of dorsal-root ganglia and sensory innervation of the hip in rats. J Bone Jt Surg 90-B:254–257

Nesslinger K (1996) Functional morphology of nociceptive and other fine sensory endings. Prog Brain Res 113:273–298

Peters A, Palay SL, Webster F (1976) The fine structure of the nervous system: the neurons and supporting cells. W.B. Saunders Company, Philadelphia, pp 90–117

Ramón y Cajal S (1904) Textura del Sistema Nervioso Central del Hombre y Los Vertebrados. Luis Moya editor, Madrid

Roy CS, Sherrington CS (1890) On the regulation of blood supply of the brain. J Physiol 11:85–108
Sánchez-Islas E, León-Olea M (2001) Nitric oxide synthase inhibition during synaptic maturation decreases synapsin I immunoreactivity in rat brain. Nitric Oxide 10:141–149
Sandel JH (1986) NADPH diaphorase histochemistry in the macaque striate cortex. J Comp Neurol 251:388–397
Sharp FR, Kauer JS, Shepherd GM (1975) Local sites of activity-related glucose metabolism in rat olfactory bulb during olfactory stimulation. Brain Res 98:596–600
Sherrington CS (1892) Note toward the localization of knee-jerk. Br Med J 1:545
Silverman JD, Kruger L (1990) Selective neuronal glycoconjugate expression in sensory and autonomic ganglia: relation of lectin reactivity to peptide and enzyme markers. J Neurocytol 19:789–801
Smith TK, Spencer NJ, Henning GW, Dickson EJ (2007) Recent advances in enteric neurobiology. Neurogastroenterol Motil 19:869–878
Suárez-Solá ML. González-Delgado FJ, Pueyo-Morlans M, Medina-Bolivar OC, Henandez-Acosta NC, Gonzalez-Gomez M, Meyer G (2009) Neurons in the white matter of the adult human cortex. Front Neuroanat. https://doi.org/10.3389/neuro.05.007.2009
Swanson LW (2004) Brain maps III. Structure of the rat brain. Elsevier, Amsterdam
Tasker JG, Oliet SH, Bains JS, Brown CH, Stern JE (2012) Glial regulation of neuronal function: from synapse to systems physiology. J Neuroendocrinol 24:566–576
Uddman R, Edvinsson L, Ekman R, Kingman T, McCulloch J (1985) Innervation of the feline vasculature by nerve fibers containing calcitonin gene-related peptide: trigeminal origin and co-existence with substance P. Neurosci Lett 62:131–136
Varela-Echevarría A, Vargas-Barroso V, Lozano-Flores C, Larriva-Sahd J (2017) Is there evidence for myelin modeling by astrocytes in the normal adult brain? Front Neuroanat. https://doi.org/10.3389/fnana.2017.00075. **(ISSN 16625129)**
Vargas-Barroso V, Larriva-Sahd J (2013) A cytological and experimental study on the primary olfactory afferences to the piriform cortex. Anat Rec 296:1297–1316
Vaucher E, Tong X-K, Cholet N, Lantin S, Hamel E (2000) GABA neurons provide a rich input to microvessels but not nitric oxide neurons in the cerebral cortex: a means for direct regulation of local cerebral flow. J Comp Neurol 421:161–171
Ward NL, Lemana M (2004) The neurovascular unit and its growth factors: coordinated response in the vascular and nervous system. Neurol Res 26:870–883. https://doi.org/10.1179/016164104X3798
Warfvinge H, Edvisson L (2017) Distribution of CGRP receptor components in the rat brain. Cephalalgia. https://doi.org/10.1177/0333102417728873
Whitman MC, Fan W, Rela L, Rodríguez-Gil J, Greer Ch (2010) Blood vessels form a migratory scaffold in the rostral migratory stream. J Comp Neurol 516:94–104. https://doi.org/10.1002/cne.22093
Xu F, Greer Ch A, Shepherd GM (2000) Odor maps in the olfactory bulb. J Comp Neurol 422:489–495
Zhang L, Lin P, Pan J, Yuanyuan M, Wei Z, Jiang L, Wang L (2018) CLARITY for high-resolution imaging and quantification of vasculature in whole mouse brain. Aging Dis 9:262–272. https://doi.org/10.14336/AD.2017.0613
Zimmerman AG, Bai L, Ginty DD (2014) The gentle touch receptors of the mammalian skin. Science 346:950–954
Zonta M, Sebelin A, Gobbo S, Fellin T, Pozzan T, Carmignoto G (2003) Glutamate-mediated cytosolic calcium oscillations regulate a pulsatile prostaglandin release from cultured rat astrocytes. J Physiol 553:407–414